ABSTRACT

COMPTON, BRANDON THOMAS. Understanding the Behavior of a Post-Tension Rod Anchorage Mechanism in a Concrete Dam. (Under the direction of Dr. Abhinav Gupta)

Maintaining the structural integrity of hydroelectric dams is highly important due to the significant economic and physical consequences of a dam failure. However, many dams are aging and the structural strength of some has begun to deteriorate. Although many different types of dams are currently in existence, this study focuses on a specific type of dam which utilizes tainter gates to control water flow. These tainter gates transfer the hydrostatic forces into the monolithic structure of the dam through groups of post-tension rods (trunnion rods). Documented studies have revealed some of the trunnion rods on specific dams have experienced failure. The currently accepted means of testing the tension of a trunnion rod is through a lift-off test. However, the hazard, cost, and time requirement of such tests make the testing method an undesirable long-term solution. As such, the United States Army Corps of Engineers (USACE) is currently investigating whether the Dispersive Wave (DW) Non-Destructive Test (NDT) could be utilized as a preferred testing method instead of the lift-off testing method. However, more research is needed to validate the applicability of the DW testing method. As such, the focus of this study is to provide a detailed description of the DW testing method, evaluate the limitations of existing finite element (FE) modeling methods, and propose an alternative FE modeling method to address these limitations. In addition, a simplified FE model is presented utilizing a rotational stiffness for the trunnion rod anchorage mechanism. The effects of a variable rotational stiffness and tensile load on the natural frequency of the trunnion rod are also investigated.

Understanding the Behavior of a Post-Tension Rod Anchorage Mechanism in a Concrete Dam

by
Brandon Thomas Compton

A thesis submitted to the graduate faculty of
North Carolina State University
in partial fulfillment of the
requirements for the Degree of
Master of Science

Civil Engineering

Raleigh, North Carolina

2015

APPROVED BY:

_____	_____
Dr. Rudolf Seracino	Dr. Mohammad Pour-Ghaz

_____
Dr. Abhinav Gupta
Chair of Advisory Committee

DEDICATION

To my wife, Emily.

BIOGRAPHY

Brandon Compton was born in Greenville, SC but grew up in Charlotte, NC. He began attending undergraduate studies at North Carolina State University in August, 2006. After receiving a Bachelor of Science degree in Civil Engineering in May, 2010, Brandon wanted to pursue additional education, but felt it was important to gain experience in the field that would prepare him for a deeper understanding of graduate studies. He began working at FDH Engineering (now known as FDH Velocitel) as a Project Engineer designing and analyzing telecommunication towers, water tanks, rooftop structures, and foundations in June, 2010. After four years of employment, Brandon was promoted to Project Engineer III, leading a team of younger engineers in one of the more challenging regions to manage.

After two years of experience, Brandon decided to begin pursuing graduate studies part time while working to improve his engineering knowledge. Once accepted into the graduate program at NC State University, Brandon met with Dr. Abhinav Gupta to discuss his desire to pursue research despite working full time. Aware of the high priority his employer, FDH Velocitel, placed on research, Brandon met with executives within the company to see if research opportunities were available. As a result of the meeting, this research project came to fruition.

Brandon is currently employed at FDH Velocitel and due to his research efforts, Brandon was asked to join the FDH Velocitel research and development department in his current position as a Research Engineer III. In addition, Brandon currently holds a professional engineering license and is actively pursuing a structural engineering license.

ACKNOWLEDGMENTS

Many individuals were influential in the progression and conclusion of my research endeavors. I would like to express my sincerest gratitude to my advisor, Dr. Abhinav Gupta. Without his constant support, guidance, and technical expertise, this research would not have been possible. I would also like to thank Dr. Rudolf Seracino and Dr. Mohammad Pour-Ghaz for agreeing to take part in my committee and having confidence in the research work to which I have been committed.

Additionally, I would like to thank Dr. Robert Lindyberg and Christopher Murphy for providing me with the opportunity to pursue this research work and believing in my talent and abilities as an engineer. Furthermore, I would like to thank Dr. Shane Boone, Dr. Mark Cesare, Dr. Afshin Karshenas, and Jeff Cohen for the technical expertise each provided at different points during my research.

Personally, I would like to extend my gratitude to many of my family and friends for their support, patience, and encouragement. Specifically, I would like to thank my wife, Emily, for teaching me how to dream big, and for having patience with me during the long nights and difficult times that were a part of this journey. I would also like to thank my parents for their investment in my future many years ago, and the Lord for giving me the ability to learn and understand a small portion of the intricate world in which He created.

Finally, I would like to thank North Carolina State University and FDH Velocitel for providing me with the information and support necessary to make this research possible.

TABLE OF CONTENTS

LIST OF TABLES

LIST OF FIGURES

Chapter 1

INTRODUCTION

There are nearly 8,100 major dams in the United States, many of which were built decades ago by the United States Army Corps of Engineers (USACE), the Bureau of Reclamation, and other groups (USGS, 2014). All of these dams serve a significant purpose to their local communities. Some serve as a provider of irrigation, hydropower, and drinking water to nearby communities, while others serve as protectors against flooding for downstream cities, towns, and nuclear power plants (ICOLD, 2015; ASDSO, 2015; Harrison, 2008). However, as these dams have aged, the structural integrity of some has become compromised (Herweynen, 2011; NYSDEC, 2014). Regardless of their primary function to the local community, a dam failure would lead to a financial and human catastrophe for the nearby communities (USDHS, 2011; Triana et al., 2006). As such, preventative measures in the form of structural monitoring systems, field testing, and regular maintenance are needed to thwart such failures (Lynch & Loh, 2006; Ganelli et al., 2012). The focus of this particular study is to utilize the data available from Non-Destructive Testing (NDT) for an improved understanding of the behavior of a post-tension rod anchorage mechanism in a concrete dam.

1.1 Tainter Gate Dams

The United States Army Corps of Engineers (USACE) has a large inventory of dams that utilize gates called tainter gates responsible for pool control (Figure 1 and Figure 2)

(USACE, 2015). These gates are typically steel arcs which transfer hydrostatic forces from the upstream side of the dam through the supporting triangular lattice bracing as compressive forces. The geometry of the lattice bracing concentrates these forces into a beam called a trunnion girder which connects two neighboring tainter gates through the downstream side of the dam. The connection between the lattice bracing and the trunnion girder operates as a hinge, permitting the gate to be raised and lowered based on desired water levels (USACE, 2014). In a standard USACE design in use since approximately 1960, the trunnion girders are anchored through the use of post-tension steel rods called trunnion rods. The trunnion rods are typically arranged in groups and installed in PVC pipes filled with grout or grease (USACE, 2000). The primary function of the trunnion rods is to transfer the concentrated forces on the downstream side of the dam into the monolithic structure of the dam (Figure 3 and Figure 4). Transferring post-tension forces into the dam requires the use of an anchorage mechanism. In the case of the USACE dam of interest in this study, an insert/grip nut anchorage mechanism was utilized. The insert/grip nut anchorage mechanism uses a grip nut that bears directly on the face of a steel plate, which is bearing on the dam itself (Figure 4 and Figure 5). The grip nut is connected to the smooth (unthreaded) trunnion rod by means of an insert, which is manufactured as a single piece but may be split into two pieces to grip onto the rod (Figure 6). The internal face of the insert (where the insert grips the trunnion rod) consists of fine teeth, which bite into the rod under pressure. The external face of the insert has large threads which match the interior of the grip nut (Figure 7). When load from the rod is applied to the insert, the insert is pulled into the grip nut. As a result, the grip nut compresses the insert onto the surface of the rod, creating a strong mechanical connection.

Figure 1: Multiple tainter gates (Cesare et al., 2013).

Figure 2: Close-up of tainter gate.

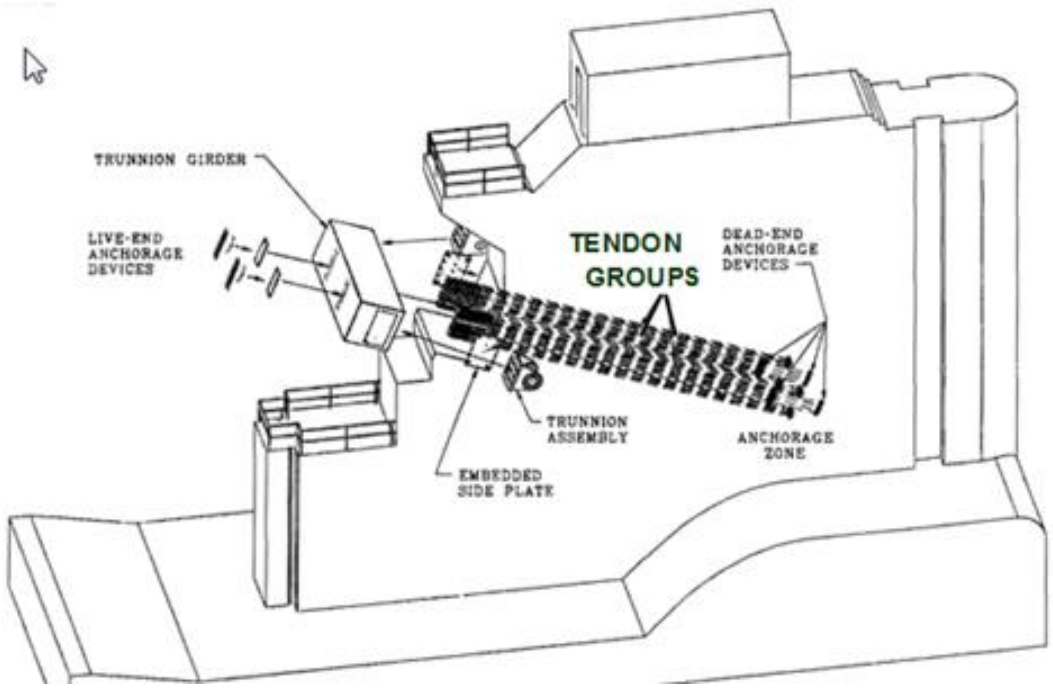

Figure 3: USACE Design for tainter gate anchorage using trunnion rods (USACE, 2000).

Figure 4: Typical group of trunnion rods with the insert/grip nut anchorage mechanism.

Figure 5: Insert/grip nut anchorage mechanism installed on a dam.

Figure 6: Insert/grip nut anchorage mechanism disassembled.

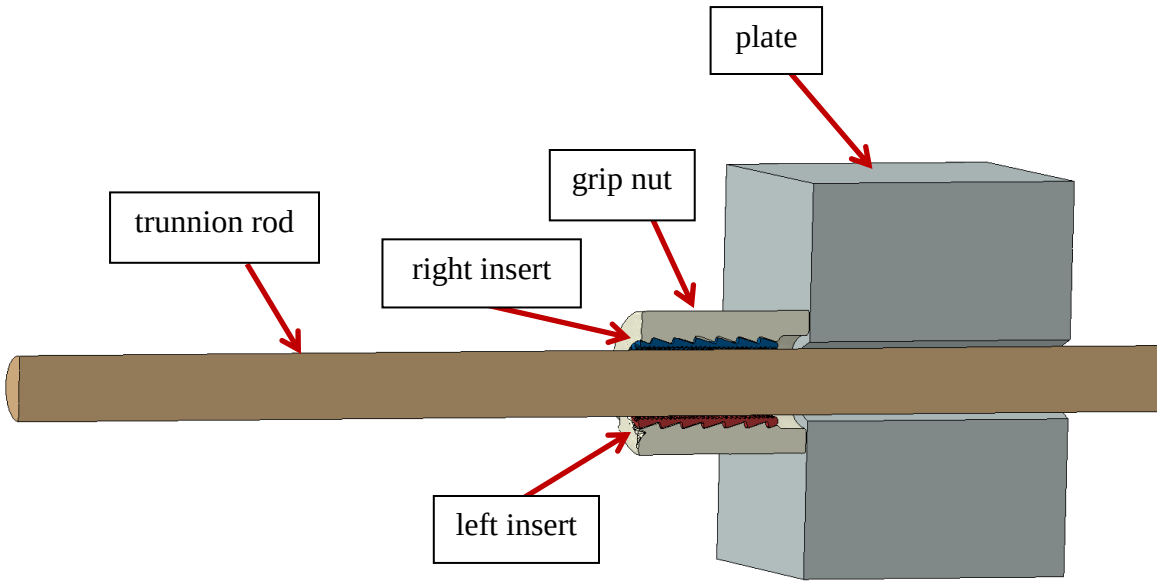

Figure 7: Cross-section of insert/grip nut anchorage mechanism.

1.2 Problem Statement

The trunnion rods in some dams have been under tension since the 1960s. In fact, some have experienced sudden rupture and damaged their cover boxes (Figure 8), while others have failed in-place unnoticed (Poiroux & Tashbin, 2009). A USACE inspection report on 14 dams with a total of 12,508 trunnion rods through the 1990s identified 156 failed trunnion rods (Schaff, 2009). Due to documented rod failures and the importance of the trunnion rods in maintaining the structural integrity of the dams, an effective testing method is needed to evaluate the in-place stress level and remaining usefulness of trunnion rods in many such dams.

1.3 Objectives

As explained later in this study, existing testing methods are limited, hazardous, costly, and time consuming. As such, a NDT method is preferred in order to improve the testing safety, cost, and time. Currently, the Dispersive Wave (DW) NDT testing method is

being researched by the USACE in conjunction with finite element (FE) modeling (Cesare & Holt, 2012; Cesare et al., 2013). However, more research is needed before this method can be fully validated. Thus, the goal of this study is to utilize the in-field data available from the DW tests on a specific dam in order to understand the behavior of the insert/grip nut anchorage mechanism. To accomplish this goal, the objectives of this particular study are fourfold.

1. Provide a detailed discussion on DW testing and existing work by other researchers on the corresponding FE analysis.
2. Propose a new FE model of the trunnion rod utilizing the insert/grip nut anchorage mechanism based on the observations from an actual anchorage mechanism to overcome the limitations of the existing FE model.
3. Confirm the validity of the proposed FE model by comparing the results with those from the DW test data for 10 different trunnion rods in which the tensile load is also known from the corresponding lift-off test.
4. Provide a simplified explanation for the behavior of the insert/grip nut trunnion rod anchorage mechanism.

1.4 Organization

This report has been divided into seven chapters. The first chapter provides an introduction to the problem being considered in this study and presents the objectives of this study. The second and third chapters provide details on existing testing methods for trunnion rods, specifically the DW testing method which is a Non-Destructive Test (NDT). In the fourth chapter, the results and limitations of prior work using FE analyses are presented. Next, the fifth chapter proposes an FE method compares results to those obtained from DW

test field data to support the accuracy of the proposed FE model. Following the presentation of the proposed FE model, the sixth chapter demonstrates how a simplified model with a rotational stiffness could be used to represent the behavior of the insert/grip nut anchorage mechanism. Additionally, simplified FE models with constant tension levels and a variable rotational stiffness, and simplified FE models with constant rotational stiffness and varying tension levels are presented. Finally, the seventh chapter provides a summary and conclusions of the results presented in the study along with a proposal for future research.

Figure 8: Trunnion rod failure via rod ejection.

Chapter 2

FIELD TESTING METHODS

There are three primary testing methods for evaluating the existing condition of a trunnion rod. The first testing method is the visual method. At times, this method is sufficient for determining if a trunnion rod has failed, but it is incapable of quantifying the existing tension in a trunnion rod. The second testing method, and the currently accepted means of evaluating a trunnion rod's in-place stress level and remaining usefulness, is a mechanical lift-off test using a hydraulic jacking system similar to the system presented in Figure 9 (Cesare & Holt, 2012). This method has the potential to damage the trunnion rods by unknowingly over-stressing them beyond their available limits, or damage the anchorage mechanism by disturbing the connection. Any such damage during the test can compromise the safety of the personnel performing the tests. Additionally, the cost and the time needed for testing (5-10 rods/day) makes the lift-off testing inefficient, particularly in dams that contain over a thousand rods. As such, a safe and economical alternative to lift-off testing is preferred. The third testing method is the NDT method. The specific NDT method currently being research by the USACE and its collaborators is the DW testing method. The DW testing method utilizes a wave based analysis technique to evaluate the existing condition of the trunnion rods without imposing additional risk of damage to the anchorage mechanisms, trunnion rods, tainter gates, or the dam itself. Due its reduced risk of damage and much greater efficiency with respect to time and cost (50-100 rods/day) (Holt et al., 2013), the DW

testing method is the preferred testing method for evaluating the existing condition of a trunnion rod. However, additional testing and validation is needed before the DW testing method can completely replace lift-off testing.

Figure 9: Typical lift-off test hydraulic jacking system setup.

Chapter 3

NON-DESTRUCTIVE DISPERSIVE WAVE TESTING

While multiple different NDT methods are available, the USACE and its collaborators are currently utilizing the DW testing method (Holt & Cesare, 2012), which has been utilized in other applications such as foundation piles (Holt & Cesare, 2010). Therefore, only this particular NDT method will be addressed in this study and is explained in the following section.

3.1 Dispersive Wave Testing

Currently, two methods are used for the DW testing on trunnion rods (Cesare & Holt, 2012a; Cesare & Holt, 2012b).

1. The first method – herein called the empirical method – uses a limited number of lift-off tests to determine the actual tension in a subset of the rods and then relates those measured tensions to a measured frequency response from DW testing to create an empirical model that relates rod frequency, diameter, cantilever length, etc. to rod tension. The empirical model is used to estimate tension for the remaining rods that have not been lift-off tested (Cesare & Holt, 2012a).
2. In the second method – herein called the FE based method – an explicit theoretical model of the rod is created, typically using a FE analysis. The FE model is used to predict the frequency response of the rod, as it varies with rod tension, diameter, cantilever length, etc. Using the FE model, actual rod tension can be estimated if the

rod frequency, cantilever length, and diameter (all measured at the dam) are known (Cesare & Holt, 2012b).

The DW testing methods have been tested on a number of dams owned by the USACE (Holt et al., 2013; Cesare et al., 2013). Testing on trunnion rods within the dam considered in this study was performed in 2013. The testing details are listed below.

1. An accelerometer was placed on the top of the exterior (cantilever) end of the trunnion rod as presented in Figure 10.
2. The cantilever end of the trunnion rod was struck with an impact device between the accelerometer and the trunnion rod anchorage mechanism (Figure 10). An emphasis was placed on using three different types of impact devices (rubber-headed mallet, wooden hammer handle, and a rubber coated steel bar) to vary the excitation frequency (Figure 11). Since the acceleration response of the trunnion rod may be more pronounced dependent upon specific rod conditions such as length, diameter, anchorage mechanism, etc., utilizing a variety of impact devices produces a wide range of excitation frequencies and increases the opportunity for gathering meaningful test data. Each impact device was used to strike the trunnion rod four times. Therefore, a total of 12 acceleration time histories of data were recorded for each trunnion rod.
3. The accelerometer set-up (consisting of piezoelectric, quartz-shear accelerometers wired to a laptop-based data acquisition system) measured the acceleration of the rod with respect to time at a sampling rate of 50,000 samples per second. Thus, the time step for the data collected was 20 micro seconds. A typical time history of

acceleration was created using the data acquired by the accelerometer and is presented in Figure 12.

4. Given the time history data, frequency spectrum data for each test was determined using Fast Fourier Transform (FFT). The results of the FFT for one such case are presented in Figure 13. The visible peaks in the data represent the natural frequencies of the significant modes in the trunnion rod. The first or fundamental frequency was calculated as an average of the values obtained from each of the 12 different impact tests on a single trunnion rod.
5. The calculated fundamental frequencies of the DW tests were paired with field measurements (cantilever length and trunnion rod diameter) and the lift-off test tension as a basis for the relationship between frequency and tension. A FE model – herein called the existing FE model – was developed to support the frequency results obtained from the DW tests.

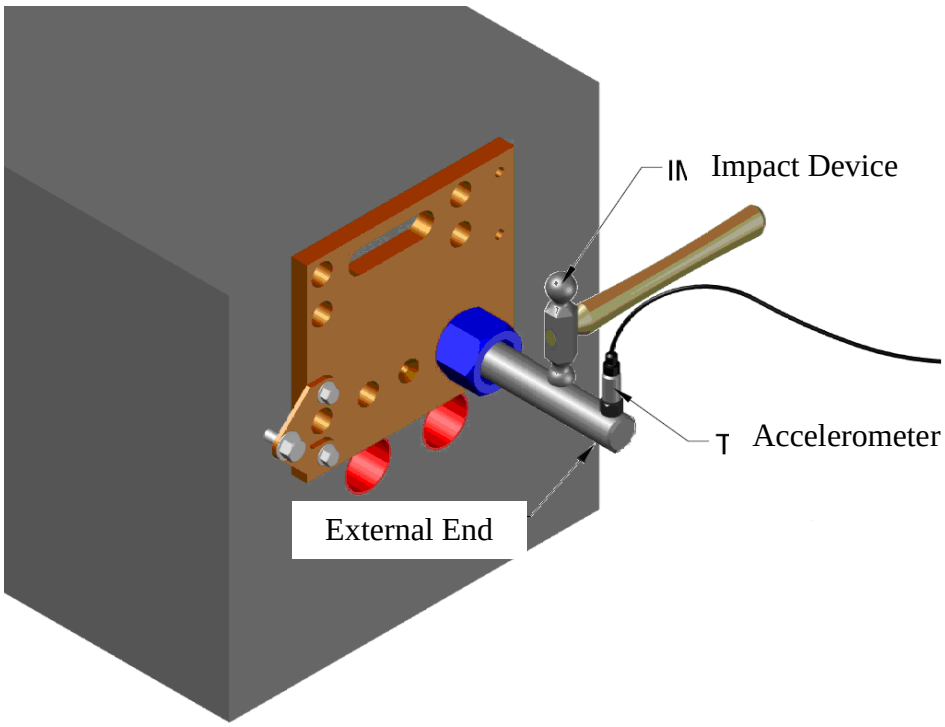

Figure 10: Diagram of the impact location with respect to the accelerometer (transducer) placement.

Figure 11: Three different types of impact devices. Rubber mallet (left), wooden hammer handle (center), and a rubber coated steel bar (right).

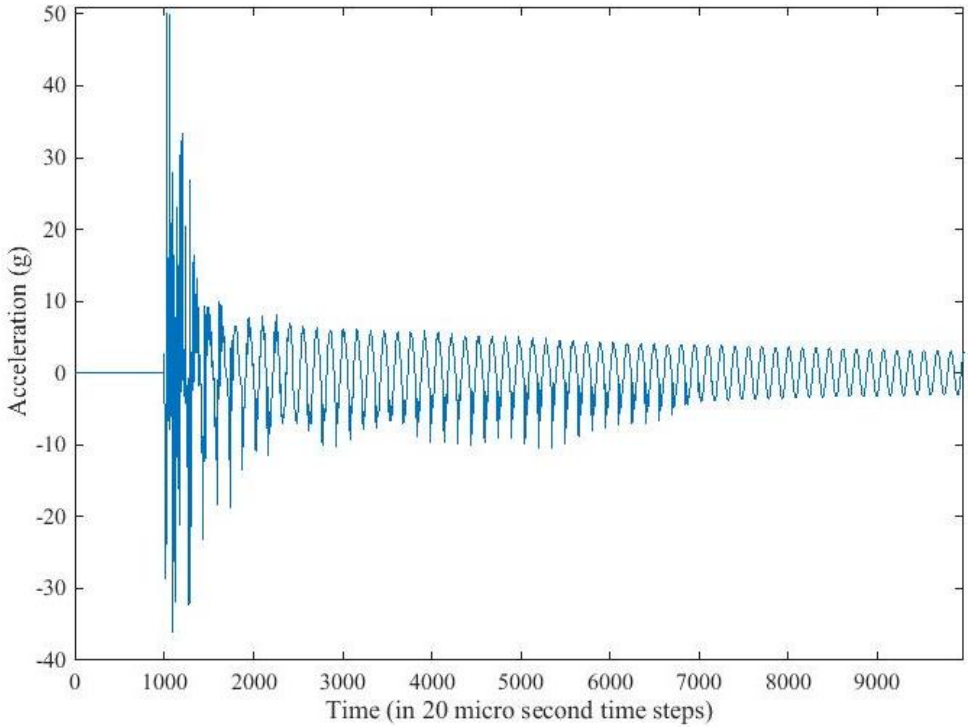

Figure 12: Time history for acceleration from one DW test.

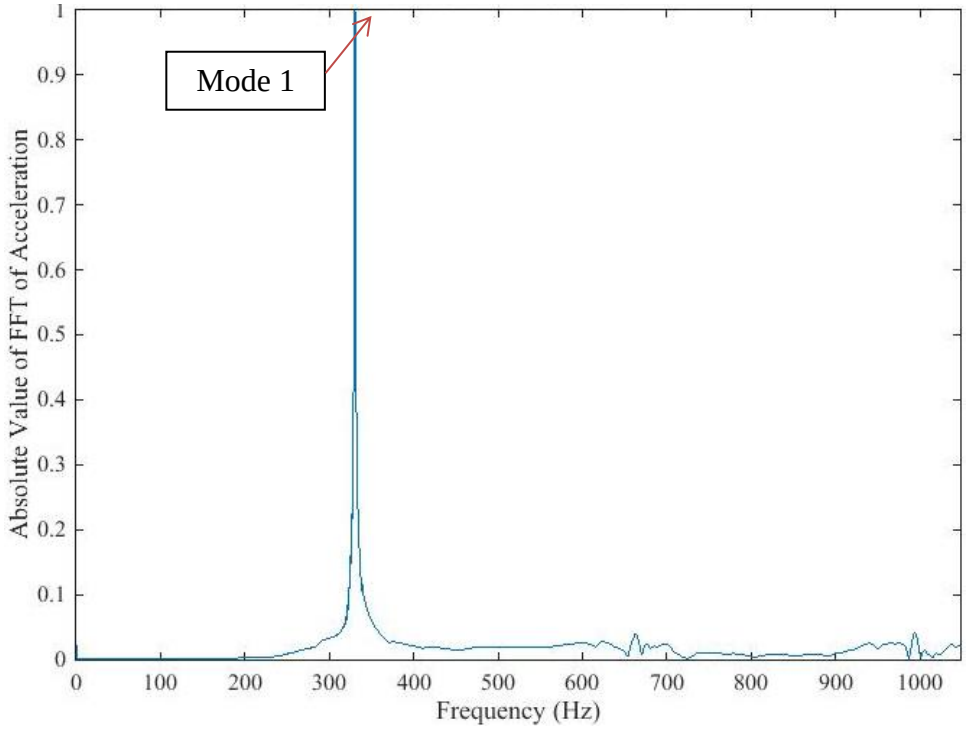

Figure 13: Frequency domain FFT from acceleration time history in Figure 12.

3.2 Recorded Data from Dam

DW tests and lift-off tests were performed on the USACE dam of interest. Additionally, field measurements of the trunnion rod diameters and cantilever lengths (distance from exterior end of the trunnion rod to the exterior end of the insert) were taken. Digital calipers were utilized to measure the diameter of the trunnion rods to an accuracy of 0.0001 inches. A tape measure was utilized to measure the cantilever length of the trunnion rods to the nearest 16^{th} of an inch. The results for the DW tests, lift-off tests, and field measurements of the trunnion rods are presented in Table 1.

Table 1: DW and lift-off test data from 10 trunnion rods.

Test Load	**Rod Dimensions**		**DW Test**
P (kip)	**D (in)**	**L (in)**	**f (Hz)**
99.2	1.2395	9.375	332.5
102.5	1.2525	9.375	328.1
107.7	1.2445	9.4375	335.1
107.8	1.2515	9.4375	333.4
104.1	1.2480	9.4375	331.8
108.0	1.2485	9.4375	332.7
103.7	1.2450	9.5	330.2
98.9	1.2410	9.5	323.1
105.5	1.2455	9.5	326.8
105.9	1.2440	9.625	325.7

3.3 Challenges

Many challenges exist that have prevented a widespread acceptance of the DW testing method. Some of the most significant challenges are listed below.

1. Since the interior (tension part) of the trunnion rod is inaccessible (Holt et al., 2013), the DW testing accelerometer must be placed on the exterior (non-tension part) of the trunnion rod. As such, the tension-dependence of the interior of a trunnion rod must

be detected through the anchorage mechanism on the tension-independent exterior of the trunnion rod.

2. Many factors affect the frequency of a trunnion rod other than the tension. Some of these are: trunnion rod diameter, cantilever length, trunnion rod condition, material properties, anchorage mechanism type, and temperature.
3. The effect of the other factors besides tension affecting the trunnion rod's frequency cannot always be accurately measured. For example, the effects of corrosion cannot be easily quantified and limited accessibility prevents accurate temperature measurements.
4. There are many types of anchorage mechanisms in existence. The insert/grip nut is only one of a few different anchorage mechanisms and each mechanism is likely to behave differently. Consequently, an understanding of one anchorage mechanism cannot necessarily be applied as a universal solution for all anchorage mechanisms.

Chapter 4

PRIOR WORK ON FINITE ELEMENT MODELING

Cesare et al. (2013) developed and proposed a three-dimensional (3D) FE model of an insert/grip nut trunnion rod anchorage mechanism. A prototype of a trunnion rod was constructed in the laboratory to allow for continual testing on an anchorage with variable loads and grouting conditions. Three significant conclusions were presented based on the results from this study. First, the study demonstrated that a 3D FE model capable of capturing the natural frequencies of the trunnion rod measured using the DW method could be developed. Second, the study demonstrated that the anchorage mechanism behaved similar to a boundary condition with a rotational stiffness that wasn't completely pinned or completely fixed. Finally, the accuracy of the FE model in capturing the cantilever frequency of the trunnion rod prototype at large tensions presented the possibility that the 3D FE model, if perfected, could serve as the alternative analysis method needed in conjunction with DW test data to estimate the tension in an existing trunnion rod. Although not explicitly stated in the report, the data presented suggests the FE model is consistently much closer to the completely fixed model and consistently less stiff than the completely fixed model across all tension levels. As such, little variation with load is observed in the FE model, demonstrating the need for more research in this area to further develop the FE model and provide understanding regarding this result.

The USACE and its collaborators conducted an additional study similar to Cesare et al. (2013) on the particular dam of interest considered in this thesis. The purpose for creating the FE model – herein called the existing FE model – was to capture the relationship between cantilever frequency and load for the insert/grip nut anchorage mechanism. The results and limitations of the existing FE model serve as the basis for this study and are presented in the next section.

4.1 Model Description

The existing FE model consists of five parts: rod, left insert, right insert, grip nut, and plate. The details of various elements used to model each of these five parts are presented in Table 2 and assembled in Figure 14. The rod and plate were constructed using 3D solid modeling techniques available in the Abaqus finite element (FE) software, specifically the Complete Abaqus Environment (CAE). However, the left insert, right insert, and grip nut parts were scanned by placing recovered parts from the field in a structured light scanner used for scanning and creating models accurate to 0.001 inches (GOM, 2014). Subsequently, the three independent models were imported into the Abaqus FE software as 3D solid models. As a result, the geometry of the scanned parts was very irregular due to the imperfections detected by the scanner. Additionally, the monolithic structure of the dam was not modeled based on the assumption that it would have a minimal effect on the results. Furthermore, since the rods are assembled in groups through a common bearing plate, the two-dimensional (2D) spacing of the rods was used to define the size of the bearing plate within the existing FE model. In regards to boundary conditions and loading, the internal end of the rod within the dam was modeled as completely fixed. Additionally, the bottom face of the plate was considered completely fixed. No additional boundary conditions were

included in the model. The load applied to the model was based on an assumed minimum and maximum expected existing tension value of 80 kips and 120 kips, respectively, and applied on the far end of the rod to simulate the post-tensioning effect.

Table 2: Details of parts used in existing FE model.

Part	Element Type	Qty. of Elements	Typical Element Size (in)
Rod	8-node, linear, hexahedron	13,860	External portion = 0.1 to 0.2 Internal portion = 5
Left Insert	10-node, quadratic, tetrahedron, modified for contact	44,500	0.05 to 0.1
Right Insert	10-node, quadratic, tetrahedron, modified for contact	43,192	0.05 to 0.1
Grip Nut	10-node, quadratic, tetrahedron, modified for contact	85,726	0.05 to 0.1
Plate	8-node, linear, hexahedron with reduced integration	565	0.4 to 0.6

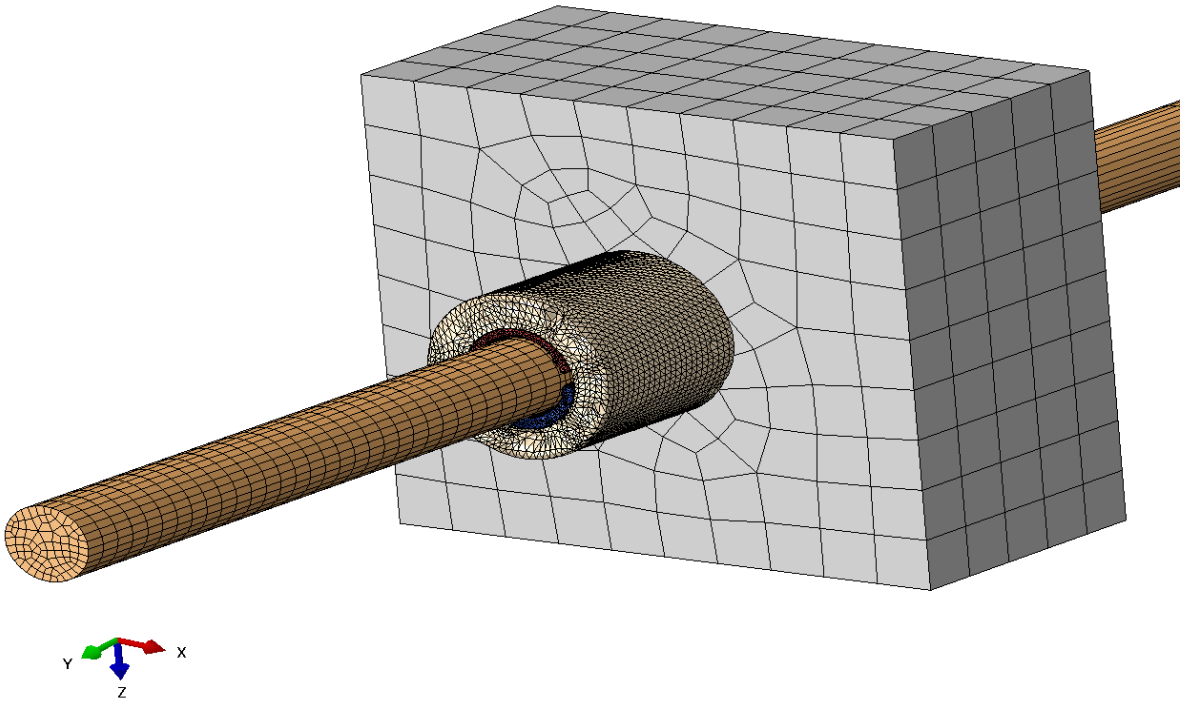

Figure 14: Insert/grip nut anchorage mechanism in the existing FE model.

4.2 Contact Surfaces

In addition to the boundary conditions and the loads applied to the existing FE model, the amount of contact and the type of contact properties defined between different parts significantly influenced the analysis and the results. In Abaqus (2013), two surfaces are considered to be in contact when the relative distance between the surfaces called "clearance" is reduced to zero. Alternatively, contact is terminated once the "clearance" between two surfaces in contact becomes greater than zero (Abaqus, 2013). In the existing FE model, there are three different contact surfaces between parts that are characterized by such a definition of contact properties (Figure 15). These are:

1. Contact surface between the grip nut and the plate
2. Contact surface between the rod and the insert pieces
3. Contact surface between the grip nut and the insert pieces

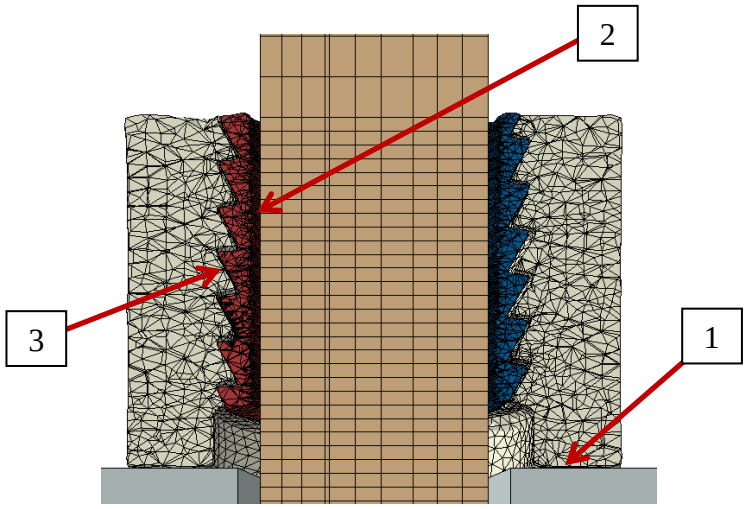

Figure 15: Visual representation of contact surfaces in the existing FE model.

Abaqus (2013) defines contact behavior between surfaces based on a "master" and "slave" relationship according to the relative size, stiffness, and mesh density of the two surfaces in contact. It recommends defining the "master" surface as the surface that is larger,

stiffer, and contains a coarser mesh. Furthermore, it is recommended that the smaller surface that is less stiff and contains a finer mesh be defined as the "slave" surface (Abaqus, 2013). In some cases, defining the surfaces based on these criteria is not straightforward and requires additional scrutiny to determine which surface could be considered as the "master" and which surface as the "slave".

4.2.1 Contact Surface between the Grip Nut and the Plate

In the existing FE model, beginning with the contact between the grip nut and the plate, the plate surface was defined as the "master" surface and the grip nut surface was defined as the "slave" surface. A "tie" constraint was used to define the relationship between the two surfaces. The "tie" constraint limits each of the nodes on the "slave" surface to have the same translational and rotational motion as the nodes on the "master" surface. As such, each of the nodes on the contact surface of the grip nut was constrained to have the same translational and rotational motion as the nearby nodes on the contact surface of the plate. With this constraint defined, frictional, compressive, and tensile forces are allowed to transfer completely between the grip nut and the plate (Abaqus, 2013).

4.2.2 Contact Surface between the Trunnion Rod and the Insert Pieces

In the existing FE model, the contact between the insert and the rod was defined in the tangential direction as "rough" friction, and in the normal direction as "hard" and separation between the contact surfaces was not allowed. "Rough" friction is defined as having an infinite coefficient of friction ($\mu=\infty$). Prior to contact, the two surfaces are allowed to translate and rotate independently. However, once contact has been established between two surfaces based on their relative proximity to each other, the surfaces stick together without sliding regardless of the magnitude of the normal force between the surfaces.

"Hard" contact is defined as allowing a compressive force of any magnitude to be transmitted between two surfaces provided they are in contact with one another. Alternatively, when two surfaces are not in contact with one another, zero force is transmitted between the surfaces. Furthermore, when two surfaces are not allowed to separate, contact remains established regardless of the magnitude and direction of the normal forces between the two surfaces. As a result, tensile forces can be transmitted across surfaces in contact when this is used as a modeling parameter (Abaqus, 2013). Since the existing FE model defines the contact behavior between the insert and the rod as "rough" and "hard" and does not allow separation once contact has occurred, the nodes on the inner surface of the insert (slave surface) are allowed to translate and rotate independently of the outer surface of the rod (master surface) until contact is established. Once contact is established, sliding and separation are completely coupled between the two surfaces throughout the duration of the analysis. Consequently, frictional, compressive, and tensile forces are allowed to transfer between surfaces regardless of their magnitude.

4.2.3 Contact Surface between the Grip Nut and the Insert Pieces

In the existing FE model, the contact between the insert and the grip nut was defined in the tangential direction as frictional (μ=0.5) using the "penalty" friction formulation, and in the normal direction as "hard" contact and separation between the contact surfaces was not allowed. The "penalty" frictional formulation allows some relative tangential motion between nodes on surfaces in contact. This motion is characterized as an "elastic slip". It is important to note that "sliding" is not the same as "elastic slip". "Sliding" occurs when the critical shear stress between surfaces in contact has been eclipsed and relative tangential motion between surfaces has initiated. Alternatively, "elastic slip" occurs when the shear

stress between surfaces is less than the critical shear stress which is defined based on the coefficient of friction and the compressive normal force between two surfaces. The magnitude of the "allowable elastic slip" can be defined as an absolute value or a percentage of the contact length between two surfaces based on a factor called "slip tolerance". The purpose of the "allowable elastic slip" is to allow for quicker convergence. As the "allowable elastic slip" approaches zero, the convergence rate decreases. Alternatively, as the "allowable elastic slip" increases, model accuracy is decreased for the sake of a quicker convergence rate. In the case of the existing FE model, the Abaqus default 0.5% "slip tolerance" was used which, according to the Abaqus (2013), is typically an acceptable balance between accuracy and convergence rate (Abaqus, 2013). The previous description of "hard" normal contact preventing separation between surfaces as it pertains to the contact behavior between the insert and the rod, also applies to the contact behavior between the insert and the grip nut. Since the existing FE model defines the contact behavior between the insert and the grip nut using the aforementioned parameters, the outer surfaces of the inserts (slave surfaces) and the inner surface of the grip nut (master surface) are allowed to translate and rotate independently of each other prior to contact. However, once contact has been initiated, compressive and tensile forces of any magnitude may be transmitted between surfaces. Additionally, frictional forces up to the critical shear stress may be transmitted between surfaces without "sliding" but with an "elastic slip" equal to 0.5% of the contact length. If the critical shear stress is eclipsed during the analysis, tangential sliding between the surfaces initiates (Abaqus, 2013).

4.3 FE Analysis Steps

In the existing FE model, a 4-step procedure was utilized to engage the friction between contact surfaces and effectively transfer the tensile load from the tensioned rods through the gripping mechanism (inserts, grip nut, and plate) and into the face of the dam, which is modeled as a fixed boundary condition on the dam side of the plate:

1. The first step in the existing FE model was to apply a displacement boundary condition to the surface or the exterior end of the inserts in order to establish contact between the inserts and the rod and between the inserts and the grip nut. This was accomplished by "kinematically coupling" the external end surfaces of the inserts to an arbitrary "control point". Effectively, this limited all of the nodes on the external end surfaces of the inserts to translate and rotate according to the rigid body motion of the "control point". The "control point" used in this step was a "reference point" which is simply a node created at an arbitrary location in 3D space. For the purposes of the existing FE model, it was used as a single node on which to apply loads and boundary conditions intended to affect the behavior of the nodes to which the "reference point" was kinematically coupled. As a result, a displacement boundary condition was placed on the "reference point" which, consequently, imposed the displacement boundary condition on the exterior end surfaces of the inserts, forcing the inserts in the axial direction of the rod toward the grip nut (Figure 16). Contact with the grip nut forced the insert into the rod, establishing contact between the four different parts. The final magnitude of the displacement boundary condition was on the order of 0.1 inches but varied with the applied tension based on results from trials to determine what was needed to engage contact.

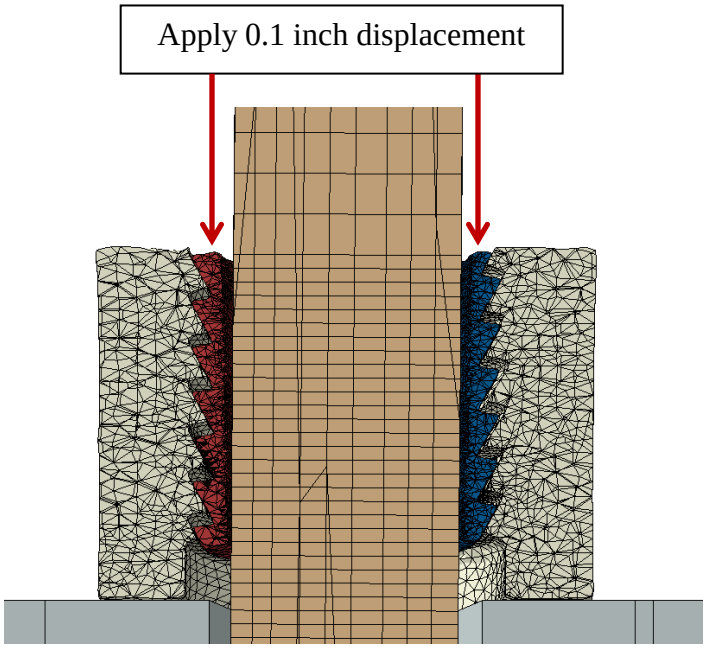

Figure 16: Step 1 of existing FE model.

2. The second step in the existing FE model was to remove the displacement boundary condition applied during step 1 and allow the bearing and frictional forces generated from the previous step to relax and achieve static equilibrium without the displacement boundary condition in step 1. The model utilizes this step to allow the system to equalize in static equilibrium prior to applying the load to the rod. The insert returns to a state of equilibrium at a location between its initial location at the beginning of the analysis and its final location at the end of step 1 (Figure 17). Additionally, the boundary conditions for the dam side of the plate and the internal end of the trunnion rod were maintained from step 1.

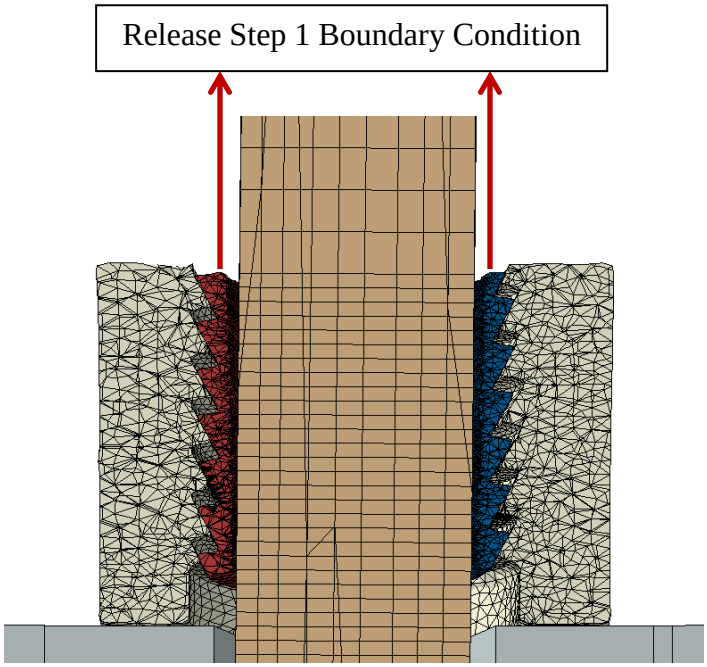

Figure 17: Step 2 of existing FE model.

3. In the third step, a static load was applied to the end of the rod within the dam (Figure 18). During this step, the axial translational boundary condition at the internal end of the rod was released and a load was applied in the same location to simulate the post-tension load within the rod.

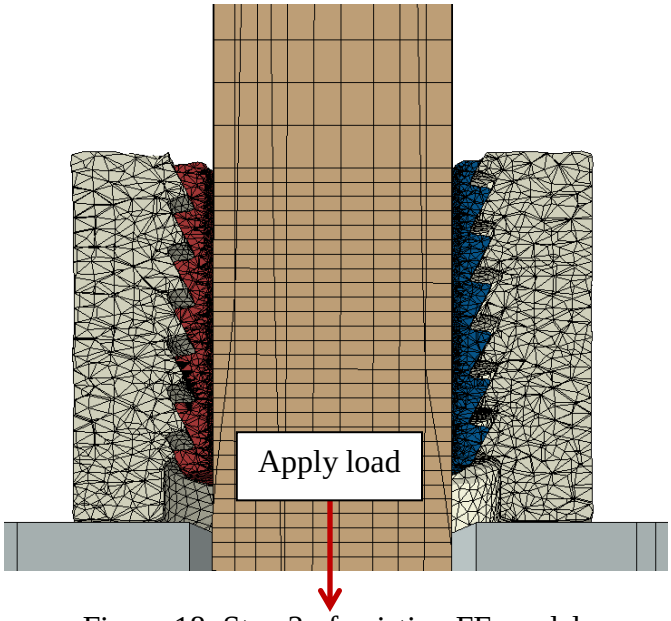

Figure 18: Step 3 of existing FE model.

4. In the final step, an eigenvalue analysis was performed to determine the natural frequencies of the system. During this step of the analysis, the model maintained the load previously applied in step 3 while reinserting the axial translational boundary condition at the internal end of the rod. The fixed boundary condition at the dam side of the plate was maintained.

4.4 Limitations

The existing FE model has some limitations which are described below.

4.4.1 Runtime Limitation

The amount of time required to perform a single analysis on a 16-core CPU with 24 GB of RAM is more than 20 hours. Such a high computational requirement makes it inefficient and impractical to conduct detailed studies for multiple load cases. Many additional FE analyses are needed to verify the model accuracy and make any necessary improvements if the FE model is to be fully validated. Additionally, even if the existing FE model, in its current state, was supported by a sufficient number of validation tests to confirm its accuracy, it would be almost impossible to use it for each rod on a dam as many dams contain hundreds, and at times thousands, of trunnion rods (Holt et al., 2013; Poiroux, 2011).

4.4.2 Scanned Part Limitation

Since the existing FE model is created by scanning recovered parts, the localized irregularities throughout different surfaces and the threads of the parts result in excessively small element sizes in order to represent the irregular surface geometry accurately. The resulting FE model consists of a very large number of irregular elements. Since scanned parts were used, any results obtained from such an analysis are highly dependent upon the nature of irregularities of a single model. Therefore, the results cannot lead to a

generalization of the understanding of the overall behavior of the insert/grip nut anchorage mechanism. Consequently, an exact comparison is not possible for each of the 10 trunnion rods described in section 3.2. Since an exact comparison is not possible for each of the 10 trunnion rods, and because the computational resources required is excessively large, only two load levels were analyzed for five different rod diameter and external length combinations; one with a load of 80 kips and one with 120 kips as shown in Table 3.

Table 3: Existing FE model results.

Tension (kips)	Diameter (in.)	External Length (in.)	Frequency (Hz)
80	1.25	9.5	312.87
120	1.25	9.5	349.97
80	1.235	9.25	307.35
120	1.235	9.25	348.20
80	1.235	9.75	275.35
120	1.235	9.75	321.42
80	1.2685	9.25	323.50
120	1.2685	9.25	367.69
80	1.2685	9.75	289.32
120	1.2685	9.75	333.51

Chapter 5

PROPOSED FINITE ELEMENT MODELING

The development of the proposed FE model was initiated as part of this study to address the limitations of the existing FE model. Specifically, the proposed FE model will accomplish the following tasks.

1. Create a FE model that captures the overall global/generalized behavior of the insert/grip nut anchorage mechanism.
2. Validate the proposed FE model rod mesh by comparing the FE results to simple beam calculations.
3. Model the exact dimensions of the ten trunnion rods with insert/grip nut anchorage mechanisms that were used for DW and lift-off testing at a USACE dam.

5.1 Proposed Simplifications

The first task of the proposed FE model was to create a model that captures the overall behavior of the insert/grip nut anchorage mechanism. Four primary changes were identified as having the potential to significantly reduce the complexity of the existing FE model and more accurately model the overall behavior of the insert/grip nut mechanism. These changes were incorporated into the proposed FE model.

1. Replace the scanned grip nut and insert parts with smooth parts built within the Abaqus FE software (version 6.13-2) CAE.
2. Simplify the contact behavior between the insert and the rod.

3. Simplify the contact behavior between the insert and the grip nut.
4. Reduce the quantity of analysis steps.

5.1.1 Scanned Part Replacement

The first change implemented in the proposed FE model was to replace the irregular surfaces of grip nut and insert parts that were created by scanning with smooth surfaces. It was proposed that the scanned surfaces used in the existing FE model added significant runtime to the model due to their irregular geometries and intricate meshes. Furthermore, the scanned parts contained surfaces with many protruding features which then required significant computational effort to represent contact behavior during the convergence process. Additionally, it is expected that each part, if scanned, would be slightly different due to manufacturing, its use, and the manner in which it was recovered. Therefore, each scan can be considered a single realization of the random variation expected in the part. As such, it is reasonable to believe that using the scanned model may not provide any additional accuracy. In fact, since the scanned model is based on a part that has already been in use and experienced plastic deformation, accuracy may be lost by modeling the plastically deformed physical part as an un-deformed part within the FEM. The aforementioned reasoning was used to justify the use of smooth surfaces.

The inserts and grip nut FE models were re-built with measurements from a set of digital calipers on the same grip nut and insert recovered from the field that was scanned in the existing FE model. Since the insert was recovered in two pieces (left and right), capturing its cross sectional measurements was possible. However, since the grip nut was recovered in a single piece, a plastic mold of the grip nut was created in order to cut the mold and measure the cross sectional dimensions. The plastic mold was created by placing the

recovered grip nut part in liquid silicone rubber and allowing it to harden. A negative of the grip nut was created once the grip nut was removed from the silicone rubber. Afterwards, liquid plastic was poured into the negative and allowed to harden to form the plastic mold. Once the plastic mold was cut in half, measurements of the grip nut cross section could be taken. The measurements for both the insert and grip nut were taken to an accuracy of 0.01 inches. Figure 19, Figure 20, and Figure 21 present the anchorage mechanism parts, grip nut silicone rubber negative, and the grip nut plastic mold.

Figure 19: Recovered insert parts within the grip nut part.

Figure 20: Recovered insert parts within the grip nut part containing a piece of a trunnion rod.

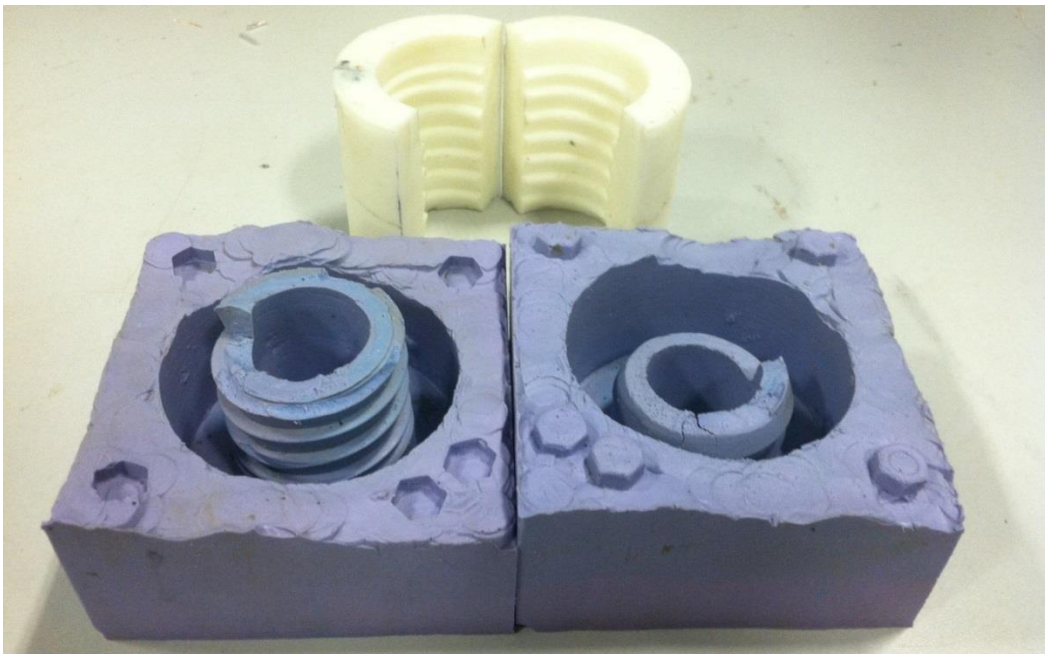

Figure 21: Silicone rubber negative and plastic mold of grip nut part cut in half.

5.1.2 Rod to Insert Contact Behavior

The second change implemented in the proposed FE model was to simplify the contact behavior between the insert and the rod. In the existing FE model, this contact behavior was defined as “rough” friction with “hard” contact and also did not allow separation between contacting surfaces once contact was established. As a result, tension, compression, and frictional forces were allowed to transmit across contacting surfaces. It was believed that this contact behavior was quite complex and increased computational time. As such, to simplify the contact behavior, it was proposed to model the interior of the insert part as smooth and completely “tie” the nodes on the interior surface of the insert (slave surface) to the exterior surface of the rod (master surface). This contact behavior is the exact same as the contact behavior previously described in detail between the grip nut and the plate in the existing FE model. Additionally, this contact behavior was justified based on the

results of a contact area test performed in parallel with this study. The contact area study involved statically loading a rod to 30 kips, 50 kips, 75 kips, 90 kips, and 105 kips and visually inspecting the segments of the rod which were gripped at different load levels to determine if the quantity and size of indentations along the rod changed as load was varied. Although it was necessary to use a slightly different anchorage mechanism (wedge/plate instead of insert/grip nut) in the contact area test since the insert/grip nut anchorage mechanism was no longer being manufactured, the geometric similarity of the interior of the insert and the interior of the wedges used in the contact area study supported the assumption that the results would be reasonably similar for both anchorage mechanisms.

The results of the contact area study revealed through visual inspection that a rod under a static load of 90 to 105 kips did not experience a significant difference in the quantity or size of the indentations on the surface of the rod due to the teeth on the interior of the wedge. Additionally, the contact area study revealed that there were no longitudinal scratches along the rod which would have indicated a slip in the connection. Ultimately, the results of the study demonstrated that a mechanical bond was maintained along the length of the wedge without sliding within a loading range of 90 to 105 kips. These results support the simplified contact behavior between the insert and the rod proposed in the proposed FE model. Also, due to the decision to use the tied connection, modeling the insert as two separate pieces was assumed to not be a significant contributor to the behavior of the connection any longer. Thus, the insert was modeled as a single complete piece in the proposed FE model. Figure 22 presents pictures of the deformed rod segments tested in the contact area study for 90 kips and 105 kips.

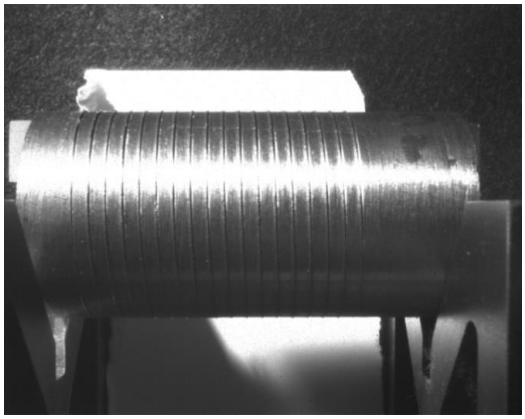

a.) 90 kip upper test rod piece.

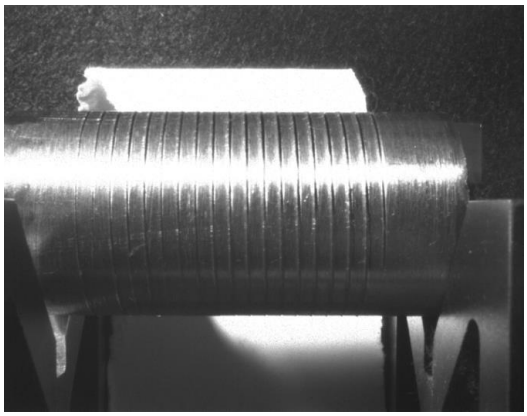

b.) 90 kip lower test rod piece.

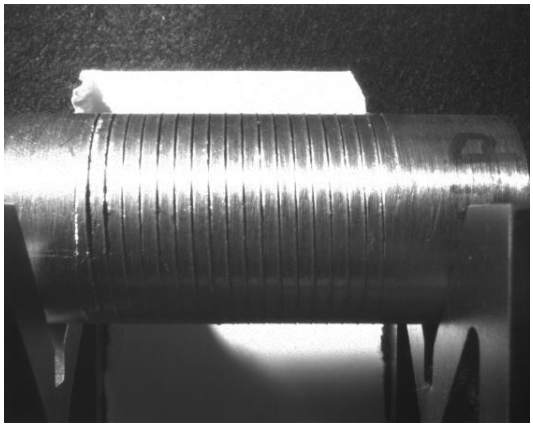

c.) 105 kip upper test rod piece.

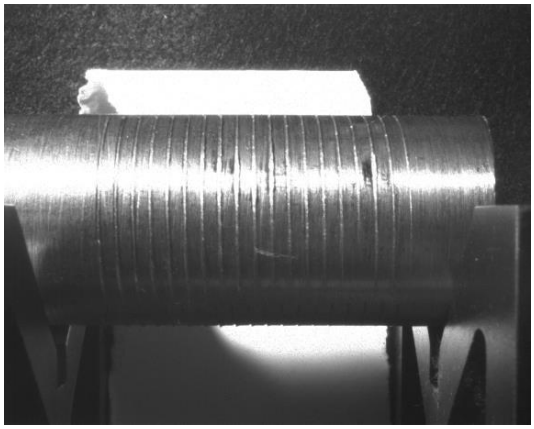

d.) 105 kip lower test rod piece.

Figure 22: Upper and lower test rod pieces loaded to 90 kips and 105 kips.

5.1.3 Rod to Grip Nut Contact Behavior

The third change implemented in the proposed FE model was to simplify the contact behavior between the insert and the grip nut. In the existing FE model, this contact behavior was defined as frictional (μ=0.5) using the "penalty" friction formulation, and in the normal direction as "hard" contact without allowing separation between the contact surfaces. It was believed that this contact behavior was more complex than necessary, possibly inaccurate, and increased computational time. As such, to simplify the contact behavior, it was proposed to model the contact behavior between the outer surface of the insert (slave surface) to the

inner surface of the grip nut (master surface) as "frictionless" with "hard" contact that allowed separation between the contact surfaces. Essentially, sliding was allowed under any magnitude of normal force, and when the two surfaces were not experiencing compressive forces, they were allowed to separate. As a result, only compressive forces were allowed to transmit across the two surfaces in contact. The basis for this proposed contact behavior was primarily to reduce complexity until additional complexity could be justified through experimental data.

5.1.4 Reduction in Analysis Steps

The fourth change implemented in the proposed FE model was to reduce the number of analysis steps. The existing FE model contained four analysis steps as detailed previously in this study. Since the primary purpose of the first two steps of the existing FE model was to establish contact between the rod, the inserts, and the grip nut, these two steps were no longer needed. Consequently, the first two steps of the existing FE model were eliminated in the proposed FE model and the remaining two steps are detailed below.

1. A static axial load was applied to the interior end of the rod within the dam. During this step, the axial translational boundary condition at the interior end of the rod within the dam was released and a static axial load was applied in the same location to simulate the post-tension load within the rod.
2. In the final step, an eigenvalue analysis was performed to determine the modal frequencies of the system. During this step of the analysis, the model maintained the load previously applied in step 1 while reapplying the axial translational boundary condition at the far end of the rod. All other boundary conditions were maintained.

5.2 Validation and Verification of Finite Element Mesh

The second task of the proposed FE model was to validate the rod mesh utilized in the proposed FE model Therefore, the grip nut, insert, and plate were removed from the proposed FE model so that only a cantilever model of the rod remained. A "reference point" was placed at the center of the rod cross section at the location along the rod where the exterior end of the insert contacted the rod – herein called the anchorage point. Next, the nodes in the same cross-sectional plane of the "reference point" were "kinematically coupled" to the "reference point". Afterwards, the "reference point" was constrained in all six DOFs to simulate a fixed boundary condition. Finally, an eigenvalue analysis was performed on the cantilever model of the rod to determine the frequencies. The fundamental cantilever frequency of the test model was compared to the fundamental frequency of a cantilever beam with an equivalent length and diameter using the classical equation for calculating the fundamental frequency of a cantilever beam as presented in equation (1) (Karnovsky & Lebed, 2001). The results of this comparison are presented in Table 4 and show that the mesh and element type (linear, 8 node, hexahedral) selected for the rod in the proposed FE model was sufficient to represent classical beam dynamic calculations within a ±0.6% error.

$$\omega_1 = \frac{1.875^2}{l^2}\sqrt{\frac{EI}{\bar{m}}} \tag{1}$$

Table 4: Results of the rod mesh validation for the proposed FE model.

Hexahedral Element Type	Classical Beam	Proposed FE Model	Comparison	
	f (Hz)	f (Hz)	Error (Hz)	%Error
Linear (Selected)	383.5	381.3	-2.2	0.6%
Linear, Reduced Integration	383.5	379.4	-4.1	1.1%
Quadratic	383.5	378.1	-5.4	1.4%

5.3 Identification of Cantilever Modes

In order to complete the final task, the proposed FE model was used to model the exact dimensions of the ten trunnion rods for which DW and lift-off testing was performed in the USACE dam of interest. These models were then used to compare the fundamental frequencies from the proposed FE models to the fundamental frequencies obtained in the DW tests. As such, ten separate proposed FE model were constructed from field measurements, lift-off testing, and DW testing for ten trunnion rods on the USACE dam of interest. The first 100 modal frequencies for each model were calculated. These modes can be categorized into three different groups.

1. Internal modes (modes identified as having a larger generalized mass indicating the larger internal portion of the trunnion rod between the internal end of the rod and the exterior surface of the plate is participating in the motion) in two orthogonal directions
2. Cantilever modes (identified as having a small generalized mass indicating primarily the smaller cantilever portion of the trunnion rod between the free end of the trunnion rod and the external surface of the plate is participating in the motion) in two orthogonal directions
3. Axial modes

Since the frequency observed in the DW testing was on the external end of the rod, the frequencies of the FE cantilever modes needed to be identified for comparison with the DW test data. Therefore, the frequencies corresponding to the cantilever modes (cantilever frequencies) were recorded. Since the cantilever length of the rod is very small compared to the internal length of the rod, the cantilever modes were quantitatively identifiable based on the mode containing the smallest quantity of generalized mass (a scalar value calculated by taking the mass matrix of the model and pre-multiplying and post-multiplying it by the eigenvector matrix of the model) as shown in Table 5 (Abaqus, 2013). Qualitatively, the cantilever modes only contained significant motion in the cantilever portion of the rod with minimal motion in the internal portion of the rod. Thus, the cantilever modes were visually identifiable in the Abaqus output based on their motion as presented in Figure 23.

Table 5: Generalized mass table from one of the ten proposed FE models used for quantitative cantilever mode identification. The smallest generalized mass values can be used to identify the two orthogonal cantilever modes.

Frequency (Hz)	Generalized Mass	Mode Type
291.2	81.04	Internal-20-X
291.2	81.03	Internal-20-Y
311.9	82.19	Internal-21-Y
311.9	80.89	Internal-21-X
327.8	1.141	**Cantilever-1-X**
328.1	1.153	**Cantilever-1-Y**
334.2	11.37	Internal-22-X
334.2	10.29	Internal-22-Y
356.1	80.65	Axial
356.1	80.63	Internal-23-X
364.5	43.92	Internal-23-Y

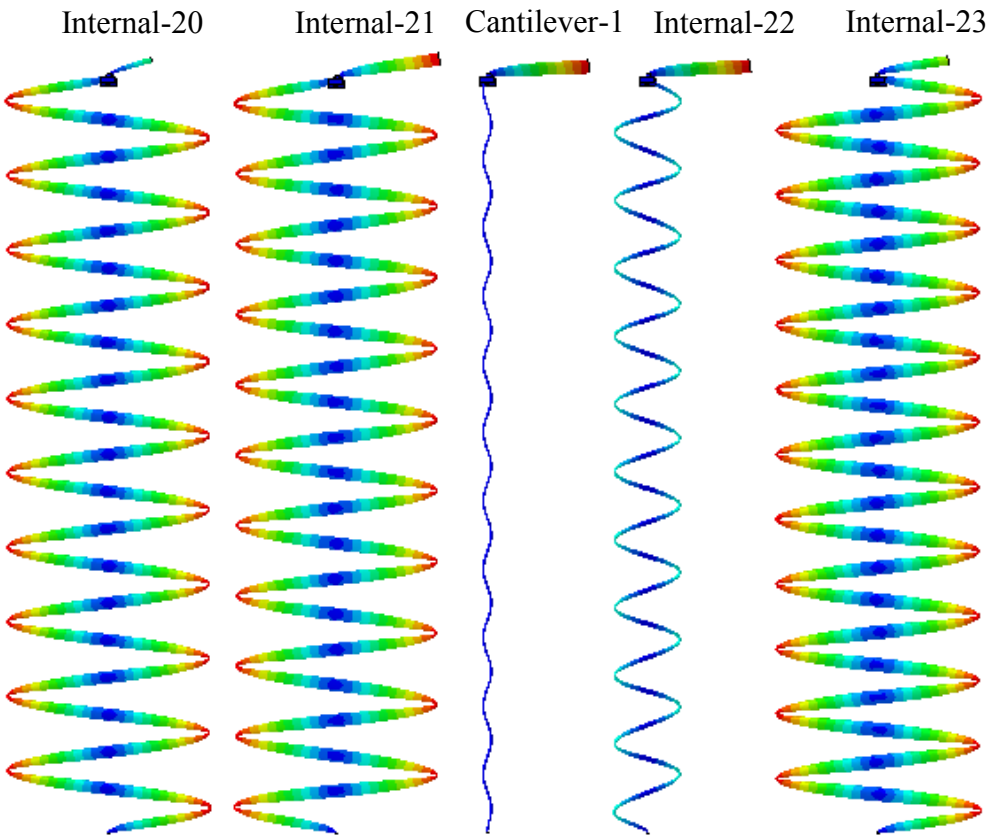

Figure 23: Visual mode shape representation from one of the FE models used for qualitative cantilever mode identification. From left to right, the mode numbers increase. The middle mode is one of the two orthogonal cantilever modes while the two modes on either side of the cantilever mode are one or two internal modes above or below the cantilever mode.

5.4 Comparison with Field Test Data

Once the fundamental cantilever frequencies were identified for each of the ten proposed FE models, they were compared with the fundamental frequencies obtained from the DW test data. A comparison of results is presented in Table 6 and Figure 24. The results of the proposed FE models show a maximum percent error of 3.2% compared to the DW test data across 10 different trunnion rod diameter, load, and cantilever length combinations. In fact, the majority of data points (9 out of 10) contained 1.6% error or less compared to the DW test data. Additionally, hand calculations using the classical fundamental frequency calculation for a cantilever beam were performed utilizing the distance from the end of the

insert and the exterior end of the rod as the length of the cantilever (Karnovsky & Lebed, 2001). The frequency results of these calculations were compared to the proposed FE model and DW test data results in Table 6 and Figure 24 and reveal the pure cantilever is consistently stiffer than the proposed FE models and the DW test data. Furthermore, the results reveal that the change in fundamental cantilever frequency of the proposed FE model is very similar to the change in the fundamental cantilever frequency of the pure cantilever. These two observations indicate the proposed FE model behaves similarly to the pure cantilever except that the rotational stiffness for the anchorage mechanism is not infinitely stiff (fixed condition). As such, additional research was performed in order to investigate whether a simplified model using a rotational stiffness could represent this behavior. Finally, the runtime of the proposed FE model is about 1.5 hours which is significantly less than the runtime of the previously developed existing FE model (20.2 hours).

Table 6: Comparison of natural frequency between proposed FE models and DW test data. Cantilever frequency hand calculations are also shown as a reference to the pure cantilever condition.

Test Load	**Rod Dimensions**		**DW Test**	**Proposed FE Model**	**Pure Cantilever**	**Results Comparison**			
P (kip)	**D (in)**	**L (in)**	**f (Hz)**	**f (Hz)**	**f (Hz)**	**Δf (Hz)**	**% Error**	**Runtime (s)**	**Runtime (hr)**
99.2	1.2395	9.375	332.5	336.2	392.2	3.7	1.1%	4569	1.27
102.5	1.2525	9.375	328.1	338.5	396.3	10.4	3.2%	4366	1.21
107.7	1.2445	9.4375	335.1	332.0	388.6	-3.1	0.9%	4414	1.23
107.8	1.2515	9.4375	333.4	333.0	390.8	-0.4	0.1%	4475	1.24
104.1	1.2480	9.4375	331.8	331.6	389.7	-0.2	0.1%	4839	1.34
108.0	1.2485	9.4375	332.7	332.6	389.8	-0.1	0.0%	4649	1.29
103.7	1.2450	9.5	330.2	328.1	383.6	-2.1	0.6%	4372	1.21
98.9	1.2410	9.5	323.1	326.9	382.4	3.8	1.2%	4467	1.24
105.5	1.2455	9.5	326.8	328.4	383.8	1.6	0.5%	4325	1.20
105.9	1.2440	9.625	325.7	320.4	373.4	-5.3	1.6%	5024	1.40

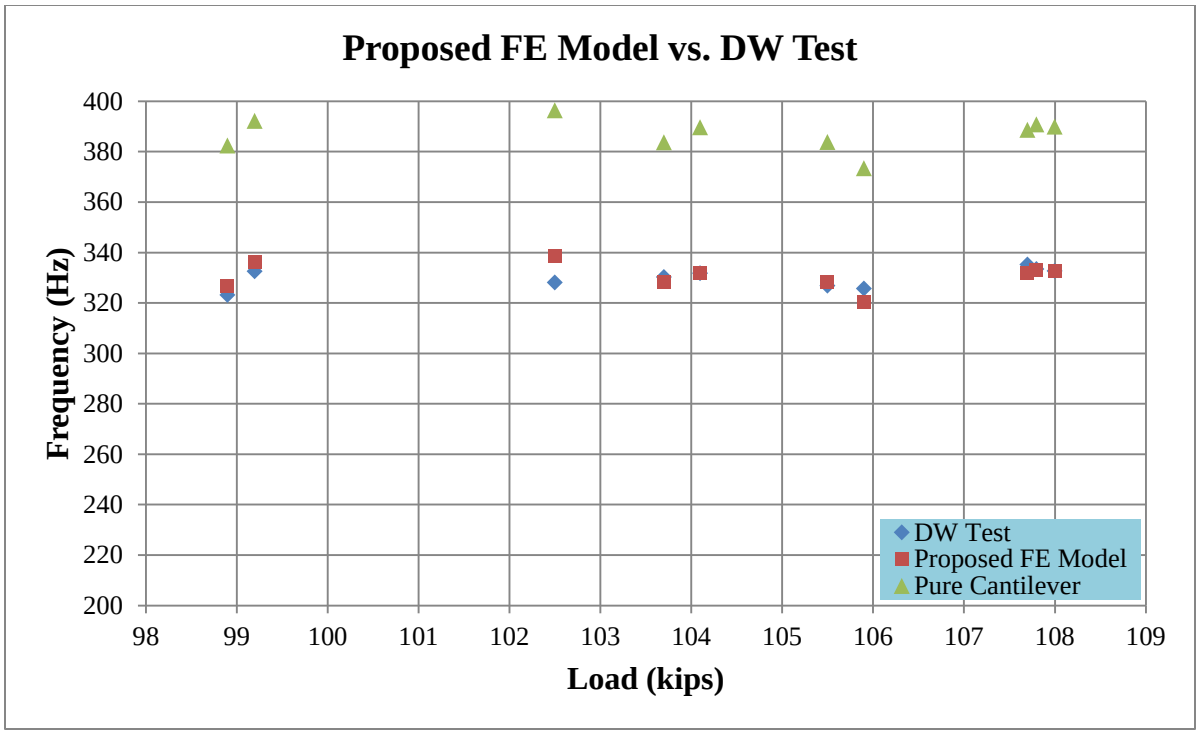

Figure 24: Comparison of natural frequency between proposed FE models and DW test data. Cantilever frequency hand calculations are also plotted as a reference to the pure cantilever condition.

Chapter 6

SIMPLIFIED FE MODEL

A simplified FE model was created to investigate whether a rotational stiffness could be used to capture the fundamental cantilever frequency results of the proposed FE models, and how the frequency of the rod would change as the internal load was increased. Figure 25 presents a visual representation of the approach used in the simplified FE model with a fixed, pinned, and variable rotational stiffness boundary condition at the anchorage point. One of the ten trunnion rods from the USACE dam of interest was selected to be modeled. The trunnion rod selected contained a 9.5" cantilever length, 1.245" diameter, and a 103.7 kip tensile load.

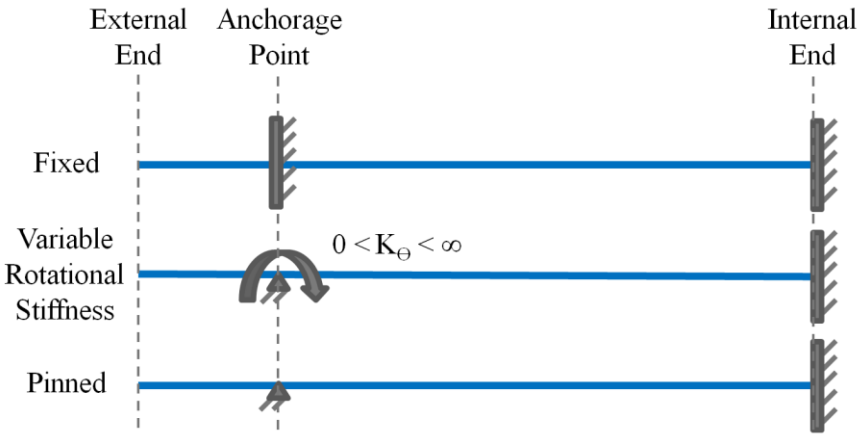

Figure 25: Boundary conditions for simplified analytical methods.

6.1 Variable Rotational Stiffness

The simplified FE model was created utilizing only the trunnion rod part. A fixed boundary condition modeled at the interior end of the rod and a variable boundary condition was modeled at the anchorage point of the trunnion rod in place of the grip nut/insert anchorage mechanism. Each analysis involved two steps. In the first step, a static, tensile load was applied at the interior end of the rod while the axial translation boundary condition on the interior end of the rod was released. This step established the existing tensile load in the rod. The second step restored the axial translation boundary condition, solved for the eigenvalue solution, and output the first 100 modal frequencies. Thirteen total simplified FE analyses were performed. Two analyses, one with the anchorage point pinned and another with the anchorage point fixed, were performed to represent the zero stiffness and infinite stiffness cases, respectively. Additionally, for the remaining eleven analyses, a pinned boundary condition with a rotational spring was applied at the anchorage point and its rotational stiffness was varied from 1 lb-in/radian to 10^{10} lb-in/radian, increasing it by a factor of 10 each time. The fundamental cantilever frequencies for each of these models were identified utilizing the method detailed previously in section 5.3 and recorded. The results of the simplified FE model utilizing a variable rotational stiffness under a constant load of 103.7 kips are recorded in Table 7 and in Figure 26 using a logarithmic scale for the x-axis containing rotational stiffness and a linear scale for the y-axis containing frequency.

Table 7: Comparison of fundamental cantilever frequency with variable rotational stiffness at the anchorage point.

Simplified FE Model	
K_Θ (lb-in/radian)	**f (Hz)**
Pinned	222.8
1.0E+00	222.8
1.0E+01	222.8
1.0E+02	222.8
1.0E+03	222.8
1.0E+04	222.9
1.0E+05	224.1
1.0E+06	280.6
1.0E+07	359.4
1.0E+08	378.7
1.0E+09	381.0
1.0E+10	381.2
Fixed	381.3

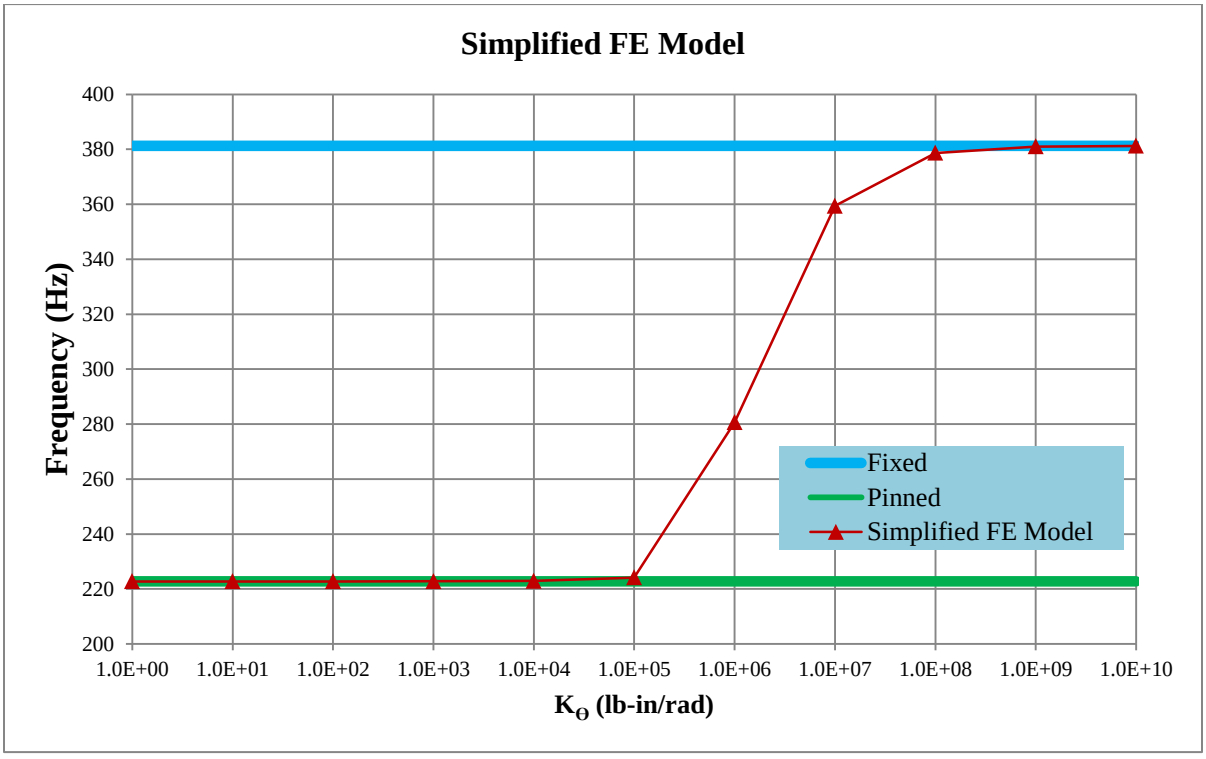

Figure 26: Comparison of fundamental cantilever frequency with variable rotational stiffness at anchorage point.

Based on the results presented in Table 7 and Figure 26, the following observations can be made concerning the fundamental cantilever frequency.

1. When the rotational stiffness at the anchorage point is less than or equal to 10^4 lb-in/radian, the frequency is within 0.1 Hz of the frequency with a pinned boundary condition at the anchorage point.
2. When the rotational stiffness at the anchorage point is greater than or equal to 10^9 lb-in/radian, the frequency is within 0.3 Hz of the frequency with a fixed boundary condition at the anchorage point.
3. When the rotational stiffness at the anchorage point is greater than 10^4 lb-in/radian and less than 10^9 lb-in/radian, the frequency varies between the frequency with a pinned and the frequency with a fixed boundary condition at the anchorage point.
4. The proposed FE model resulted in a frequency of 330.2 Hz which indicates the rotational stiffness of the insert/grip nut anchorage mechanism is between 10^6 lb-in/radian and 10^7 lb-in/radian (approximately $5x10^6$ lb-in/radian).

6.2 Modal Participation Factors and Amplification

The equation of motion for forced vibration of a structural system can be written as:

$$[M]\{\ddot{u}\} + [C]\{\dot{u}\} + [K]\{u\} = -[M]\{I_f\}a(t) \qquad (2)$$

In equation (2), [M], [C], and [K] are the mass, damping, and stiffness matrices, respectively. {u} is the displacement vector at any time t. First and second derivatives of displacement with respect to time are represented by single and double dots, respectively. a(t) is the applied acceleration at any degree of freedom such as using the impact devices in the DW test. Vector $\{I_f\}$ is an influence vector that represents the static deformation shape of

the structure when the degree of freedom where a(t) is applied is displaced by unity in the direction of a(t); i.e., vector $\{I_f\}$ is an influence line of the structure. The natural frequencies and mode shapes of vibrations are calculated by solving the eigenvalue problem:

$$[K]\{\varphi\} = \omega^2[M]\{\varphi\} \tag{3}$$

The complete displacement vector {u} can be represented as a linear combination of mode shape vectors $\{\phi_i\}$ and generalized coordinate $z_i(t)$.

$$\{u\} = \sum_{i=1}^{n} \{\varphi_i\} z_i(t) \tag{4}$$

Substituting equation (4) into equation (2) and using conditions of orthogonality, we can calculate $z_i(t)$ for each mode by solving:

$$\ddot{z}_\iota(t) + 2\xi_i\omega_i\dot{z}_\iota(t) + {\omega_i}^2 z_i(t) = \gamma_i a(t) \tag{5}$$

In equation (5), ξ_i is the damping ratio in the i^{th} mode and γ_i is the modal participation factor where:

$$\gamma_i = \{\varphi_i\}^T[M]\{I_f\} \tag{6}$$

The solution to equation (5) can be further simplified by writing:

$$z_i = \gamma_i y_i(\mathrm{t})$$

Or,

$$\{U_i\} = \gamma_i\{\varphi_i\} y_i(\mathrm{t}) \tag{7}$$

In equation (7), $y_i(t)$ is the displacement of a single degree of freedom system with identical frequencies ω_i and damping ratios ξ_i. Additionally, the quantity $\gamma_i\{\phi_i\}$ is a powerful dimensionless quantity that can be used to evaluate the significance of any mode i with

respect to its contribution to the overall response at any degree of freedom of interest. To illustrate this further, let us consider the influence vector $\{I_f\}$, which is also a deformation shape of the structure. Therefore, we can write:

$$\{I_f\} = \sum_{i=1}^{n} c_i \{\varphi_i\} \tag{8}$$

In equation (8), which c_i are constants because $\{I_f\}$ is a static deformation shape. To find c_i, we pre-multiply equation (8) by the mass matrix [M] and the modal matrix $\{\phi_i\}^T$:

$$\{\varphi_i\}^T [M]\{I_f\} = \{\varphi_i\}^T [M] \sum_{i=1}^{n} c_i \{\varphi_i\} \tag{9}$$

Invoking orthogonality, we get:

$$\{\varphi_i\}^T [M]\{I_f\} = \{\varphi_i\}^T [M]\{\varphi_i\} c_i = c_i$$

Or,

$$\gamma_i = c_i \tag{10}$$

Therefore,

$$\sum_{i=1}^{n} \gamma_i \{\varphi_i\} = \{I_f\} \tag{11}$$

For a degree of freedom at the external end of the rod, in the lateral direction of motion, the value of the element of $\{I_f\}$ is equal to unity because the external acceleration a(t) is applied at that external end. Thus, at degree of freedom k:

$$\sum_{i=1}^{n} \gamma_i {\varphi_i}^k = 1.0 \tag{12}$$

If a single mode contributes almost all the response at degree of freedom k, then:

$$\sum_{i=1}^{n} \gamma_i \varphi_i{}^k = \gamma_i \varphi_i{}^k \approx 1.0 \tag{13}$$

When multiple modes contribute, then the value of $\gamma_i\phi_i$ from a single mode is not close to unity. Often, generalized mass is also used as another parameter to identify the significant of a particular mode when mode shapes are normalized to unity and are not mass normalized. The generalized mass m_i^* in mode i can be calculated as:

$$m_i{}^* = \{\varphi_i\}^T [M] \{\varphi_i\} \tag{14}$$

6.3 Variable Internal Load

In order to understand the effect of internal load on the frequency of the rod, additional simplified FE models were created with variable internal loads and a constant rotational stiffness. Three load levels were selected (80 kips, 100 kips, and 120 kips) to be modeled using three different rotational stiffness magnitudes (K_Θ = 0 lb-in/radian (pinned), $K_\Theta = 10^5$ lb-in/radian, and $K_\Theta = 5x10^6$ lb-in/radian), totaling to nine different models. The same modeling steps and boundary conditions were used in these nine models as presented in section 6.1. Consequently, the frequencies, modal participation factors, generalized mass values, and effective mass values were output for the first 100 modes. Additionally, the eigenvector value for a node on the external end of the rod and at the center of the rod cross section for each mode was collected from the FE output. Since the 100 modes contained axial modes and modes in two orthogonal planes, it was necessary to remove all modes which were not in plane with the rotational stiffness applied to the rod. Once these modes were removed, 44 modes were found to contribute towards lateral vibrations in plane with

the rotational stiffness. Utilizing this data, three types of plots were created to evaluate the relationship between frequency and generalized mass, and the relationship between frequency and the product of the participation factor (γ) and the eigenvector value (ϕ).

1. Plots of the frequency of each mode in the x-axis and the generalized mass for each mode in the y-axis comparing the values for each of the three load levels with the same rotational stiffness in a single graph are presented in Figure 27, Figure 31, and Figure 35.
2. Plots of the frequency of each mode in the x-axis and the $\gamma\phi$ for each mode in the y-axis comparing the values for each of the three load levels and each of the three rotational stiffness magnitudes are presented in Figure 28 through Figure 30, Figure 32 through Figure 34, and Figure 36 through Figure 38.
3. Plots of the frequency of each mode in the x-axis and either the generalized mass values or the $\gamma\phi$ values in the y-axis comparing the values for each of the rotational stiffness magnitudes with the same load level in a single graph are presented in Figure 39 through Figure 44.

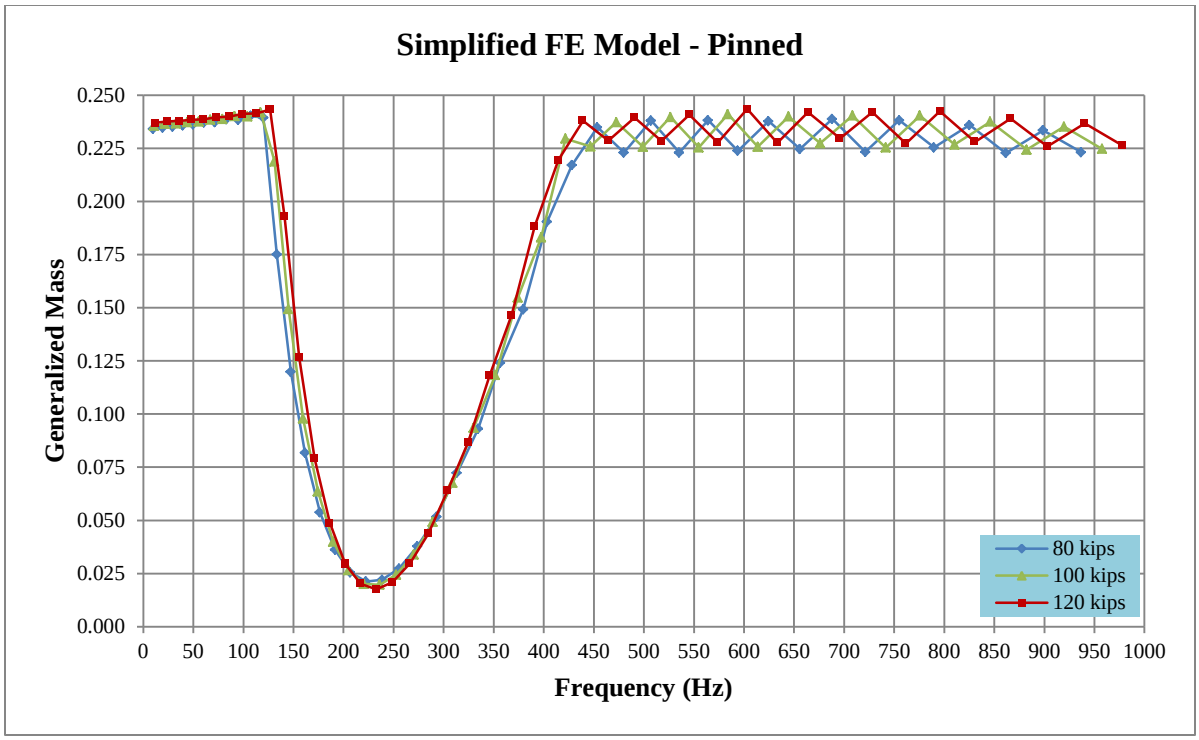

Figure 27: Generalized mass with respect to frequency for the pinned case as load varies.

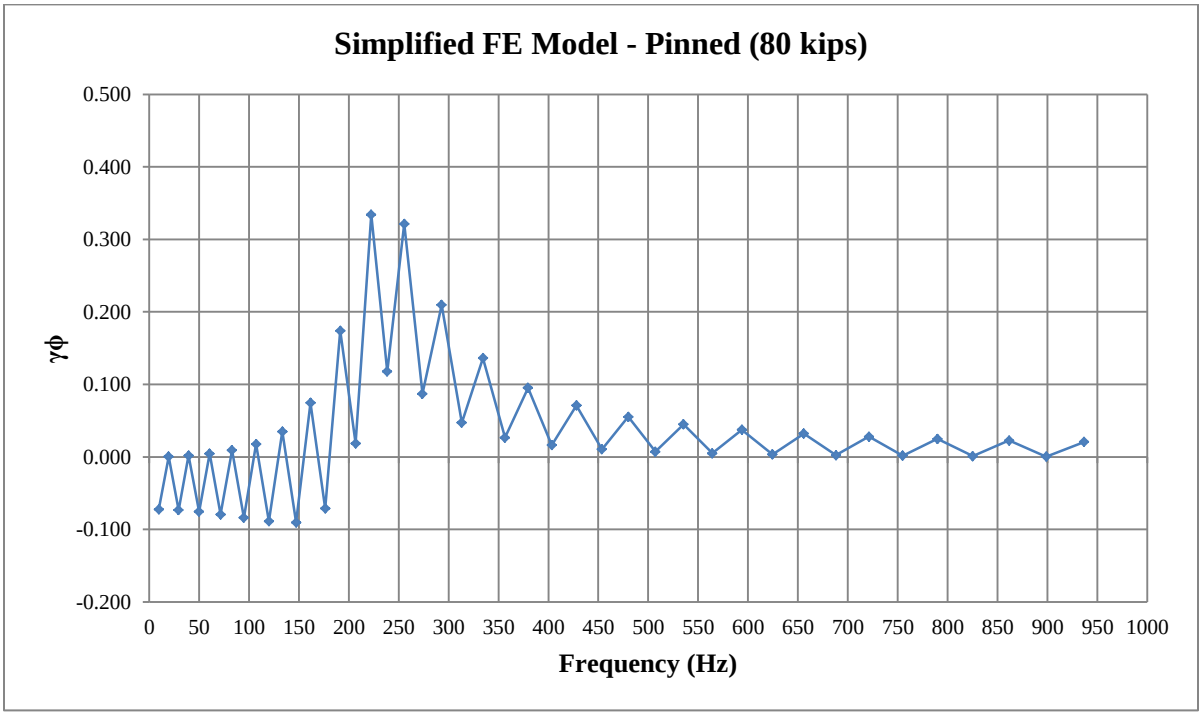

Figure 28: γϕ with respect to frequency for the pinned case at the 80 kip load level.

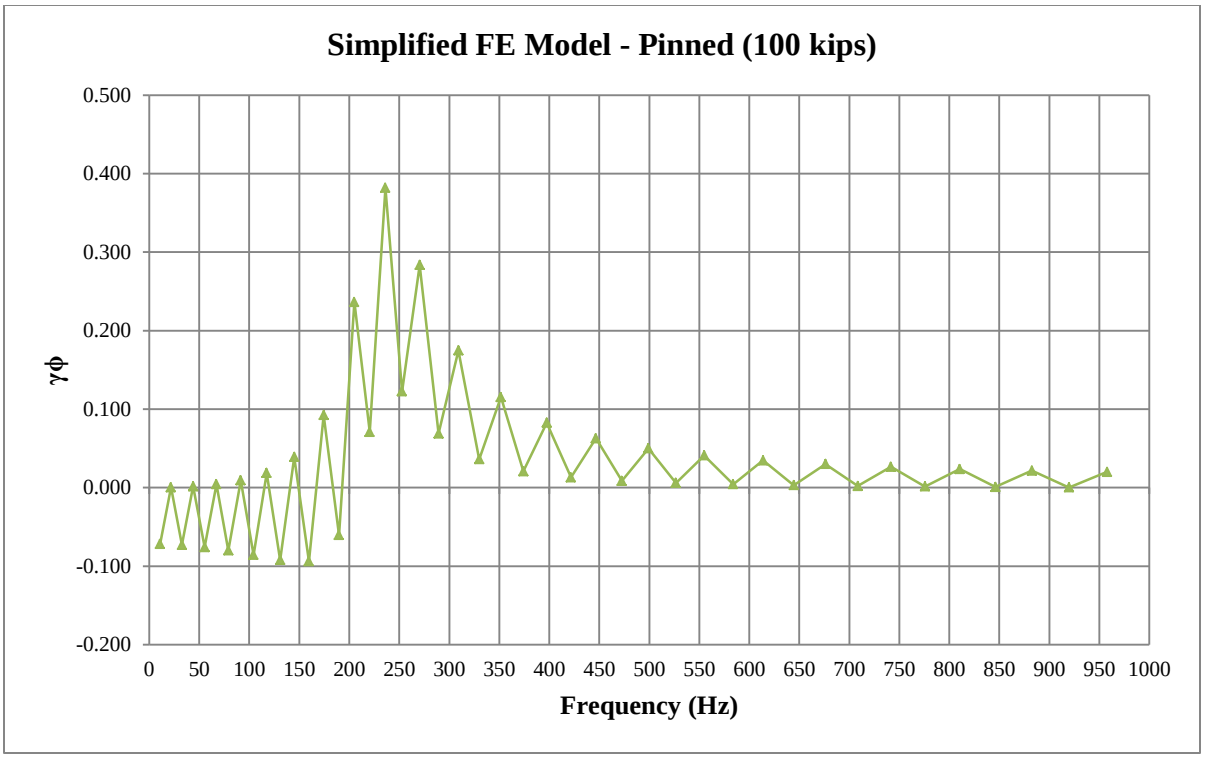

Figure 29: γϕ with respect to frequency for the pinned case at the 100 kip load level.

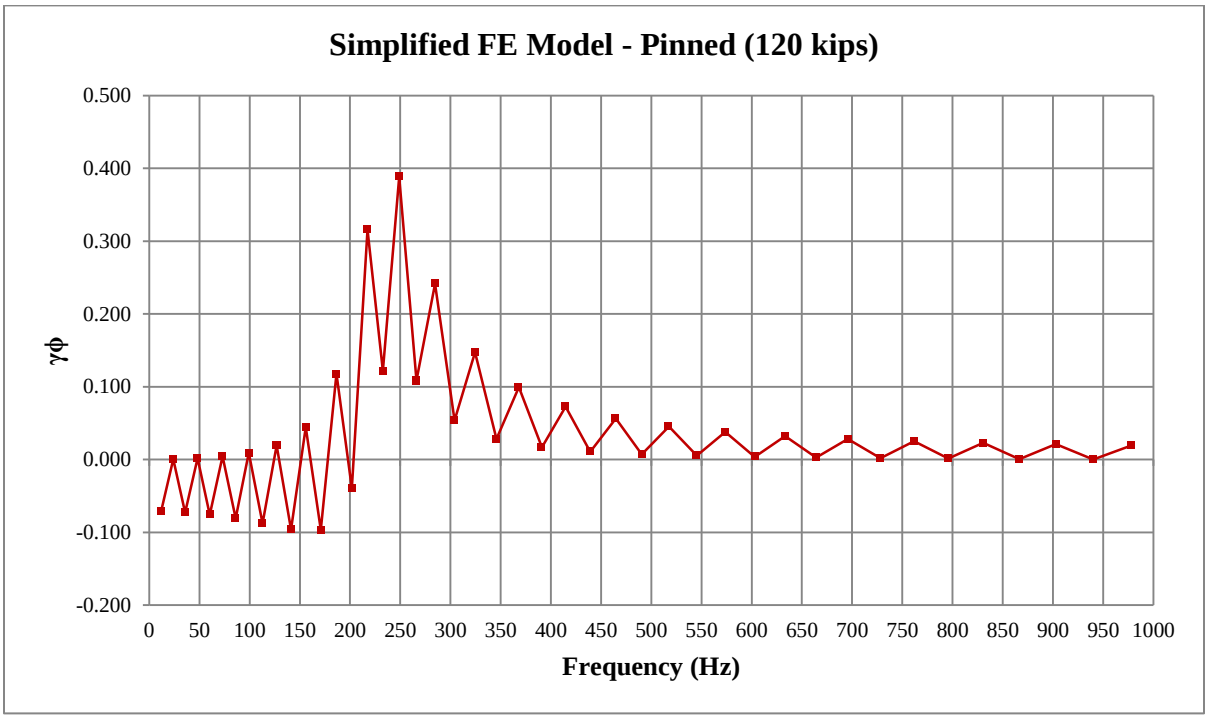

Figure 30: γϕ with respect to frequency for the pinned case at the 120 kip load level.

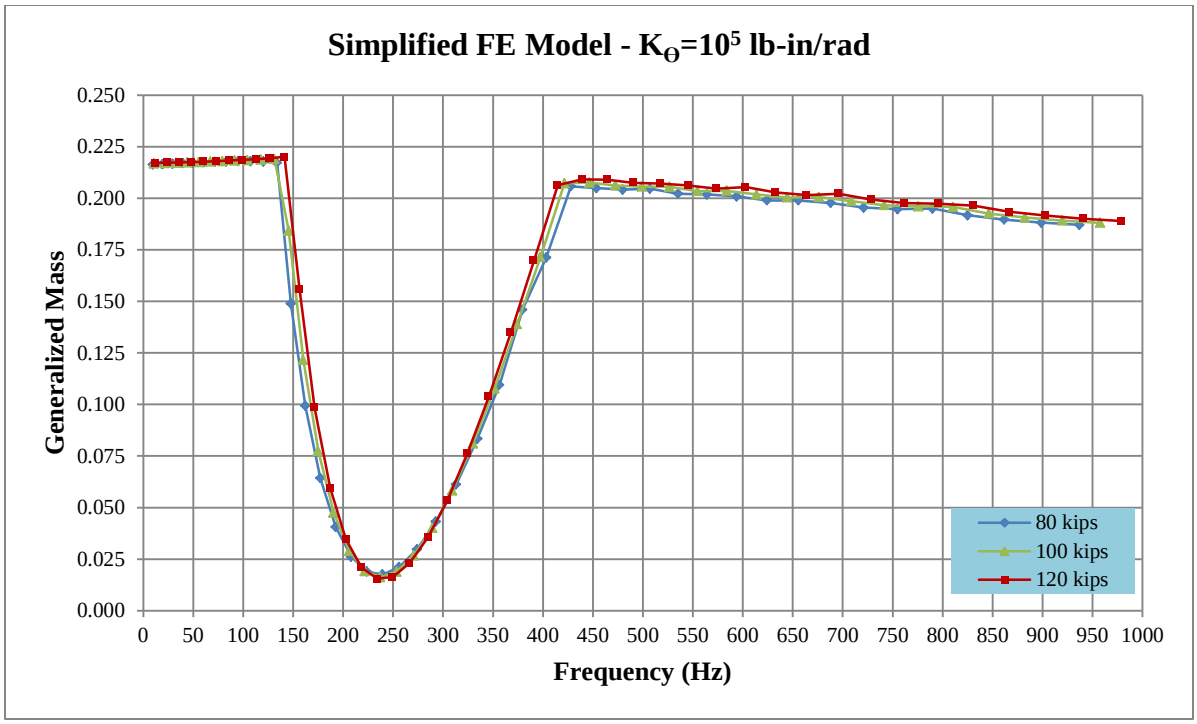

Figure 31: Generalized mass with respect to frequency for the $K_\Theta=10^5$ lb-in/rad case as load varies.

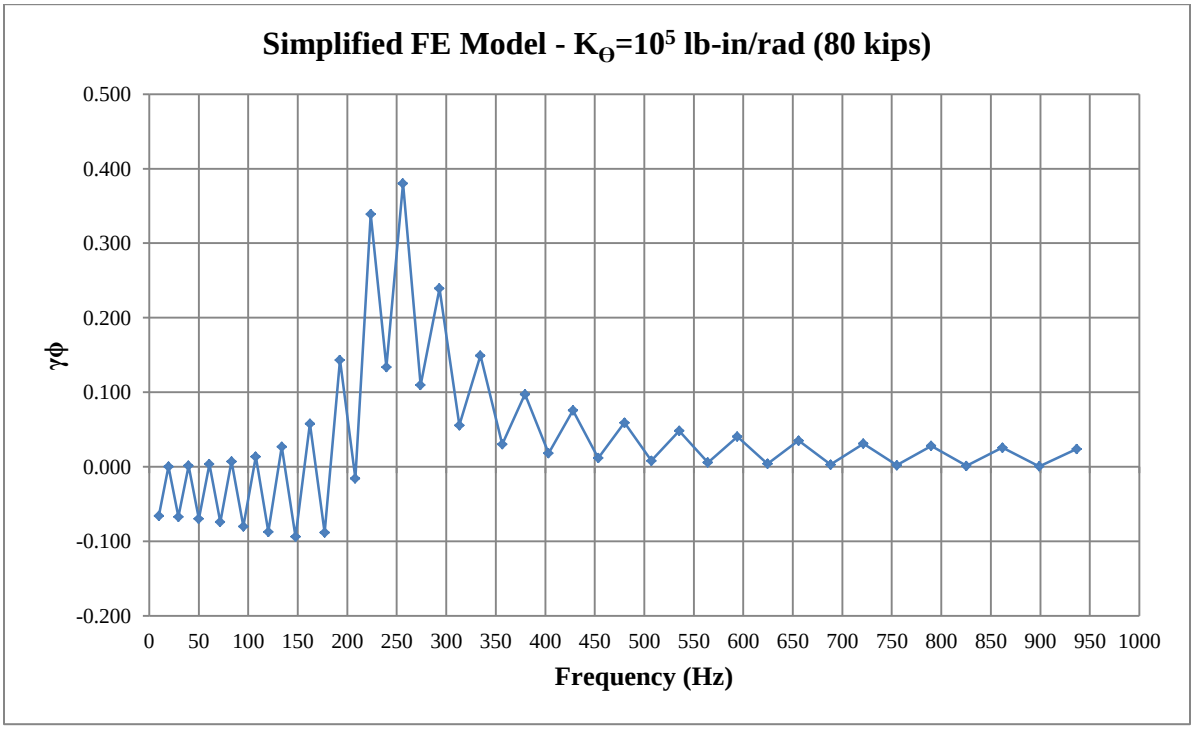

Figure 32: γϕ with respect to frequency for the $K_\Theta=10^5$ lb-in/rad case at the 80 kip load level.

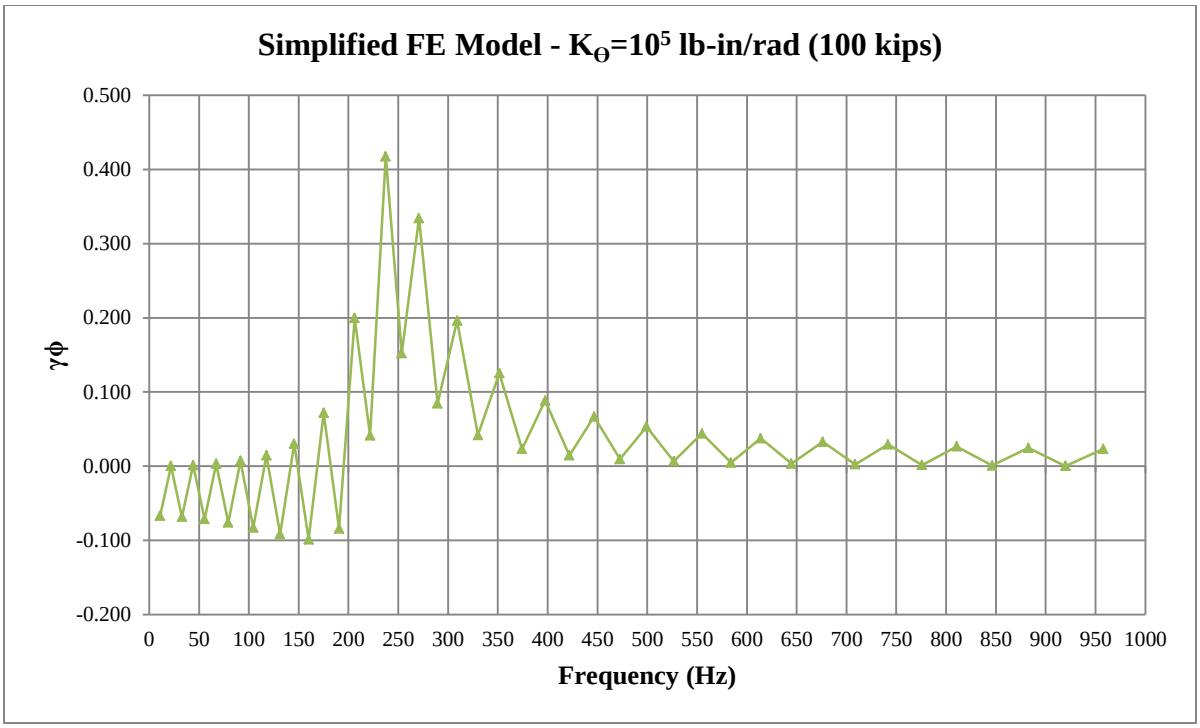

Figure 33: γϕ with respect to frequency for the $K_\Theta=10^5$ lb-in/rad case at the 100 kip load level.

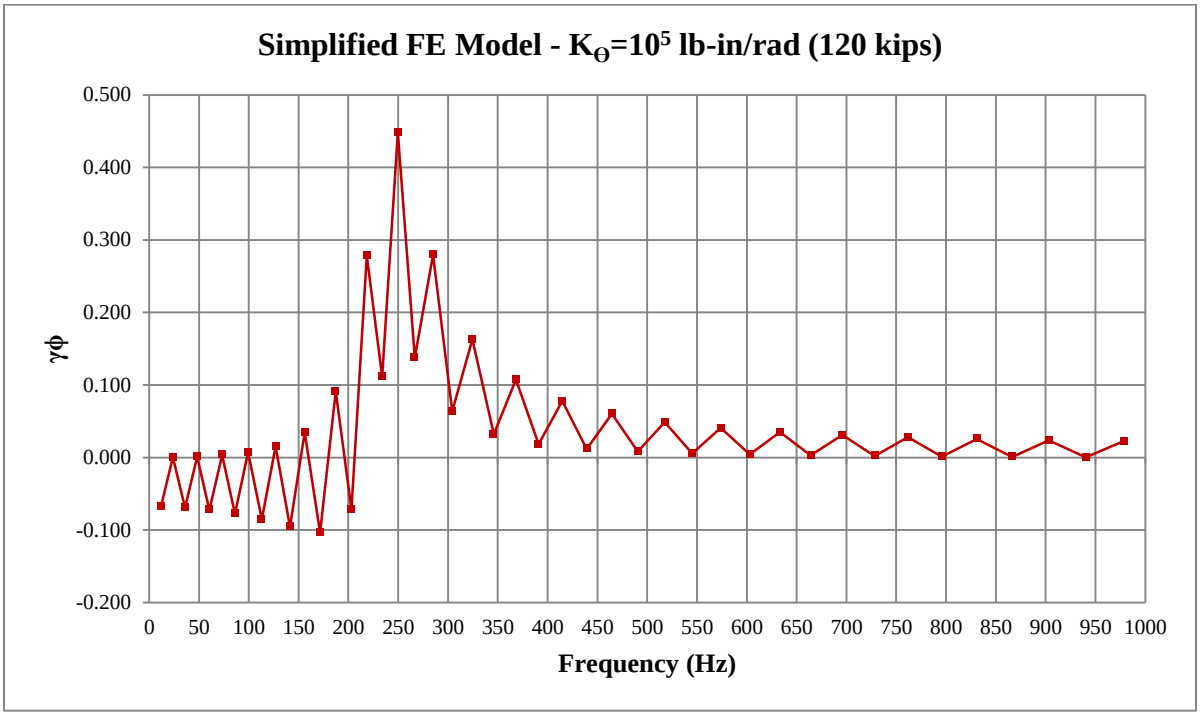

Figure 34: γϕ with respect to frequency for the $K_\Theta=10^5$ lb-in/rad case at the 120 kip load level.

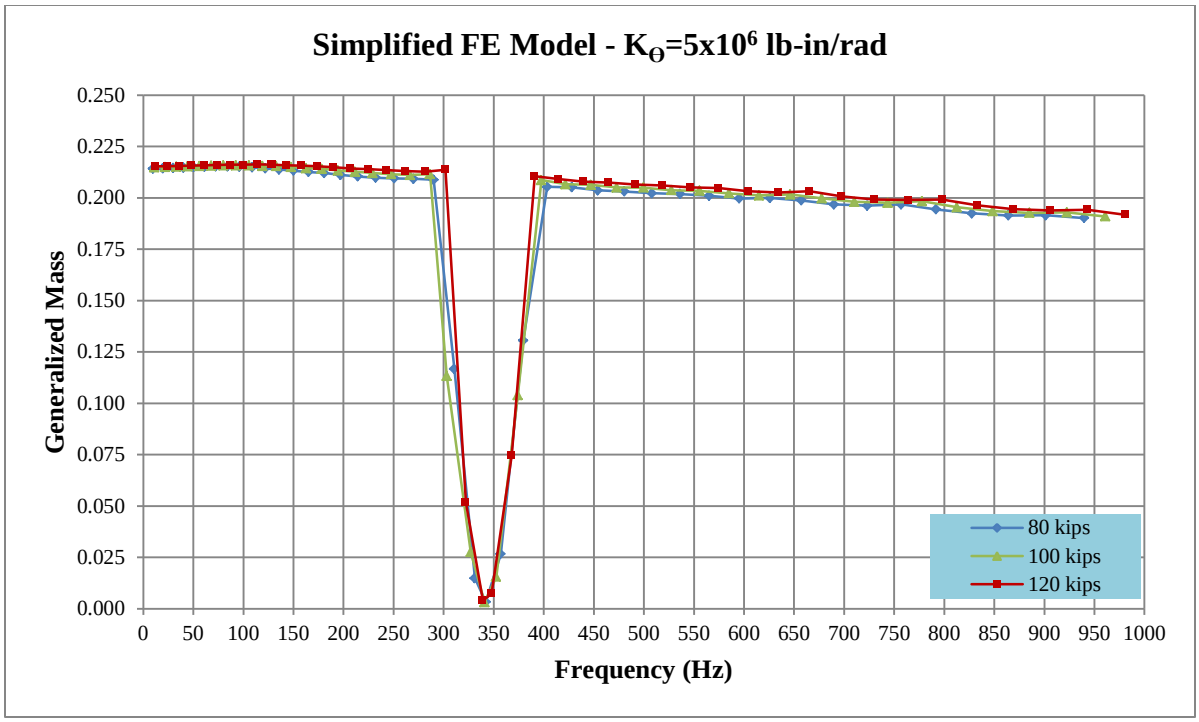

Figure 35: Generalized mass with respect to frequency for the K_Θ=5x10^6 lb-in/rad case as load varies.

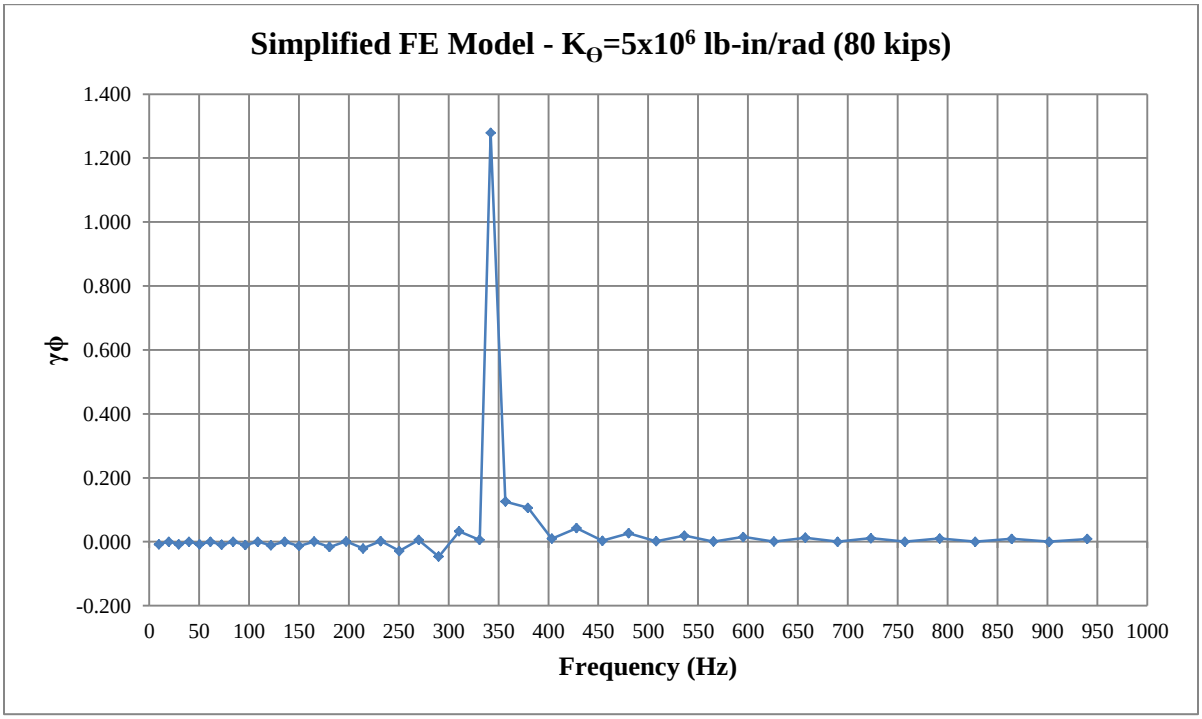

Figure 36: γϕ with respect to frequency for the K_Θ=5x10^6 lb-in/rad case at the 80 kip load level.

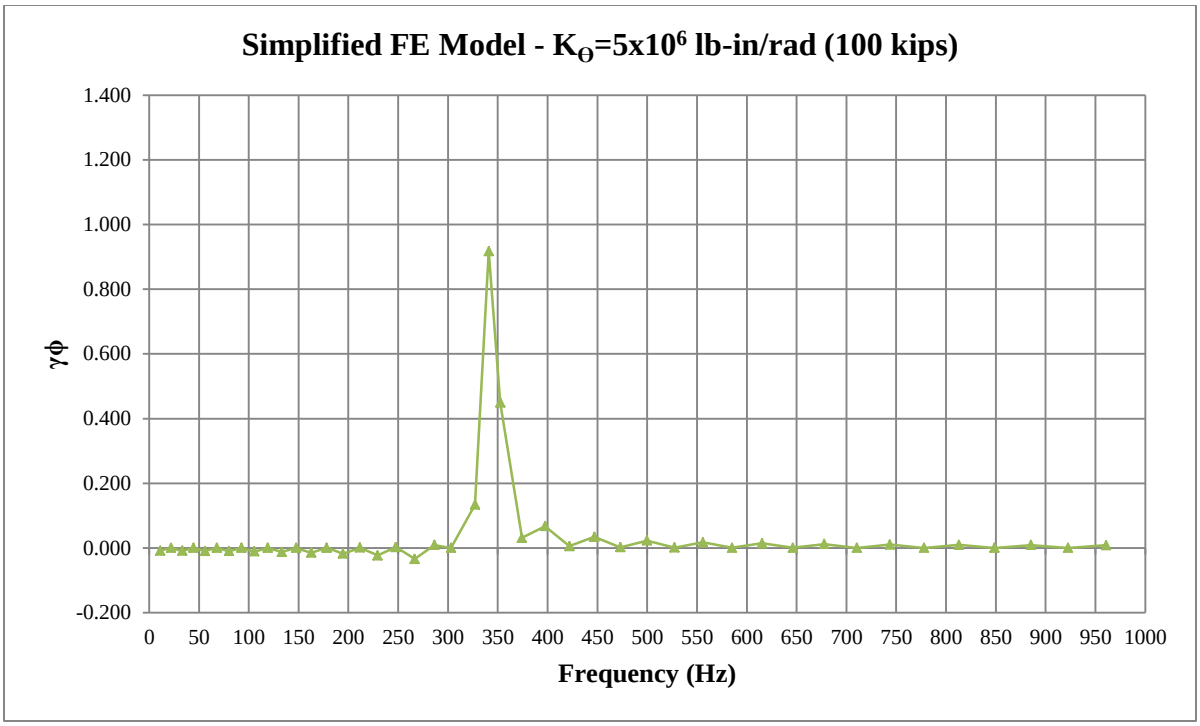

Figure 37: γϕ with respect to frequency for the K_Θ=5x10^6 lb-in/rad case at the 100 kip load level.

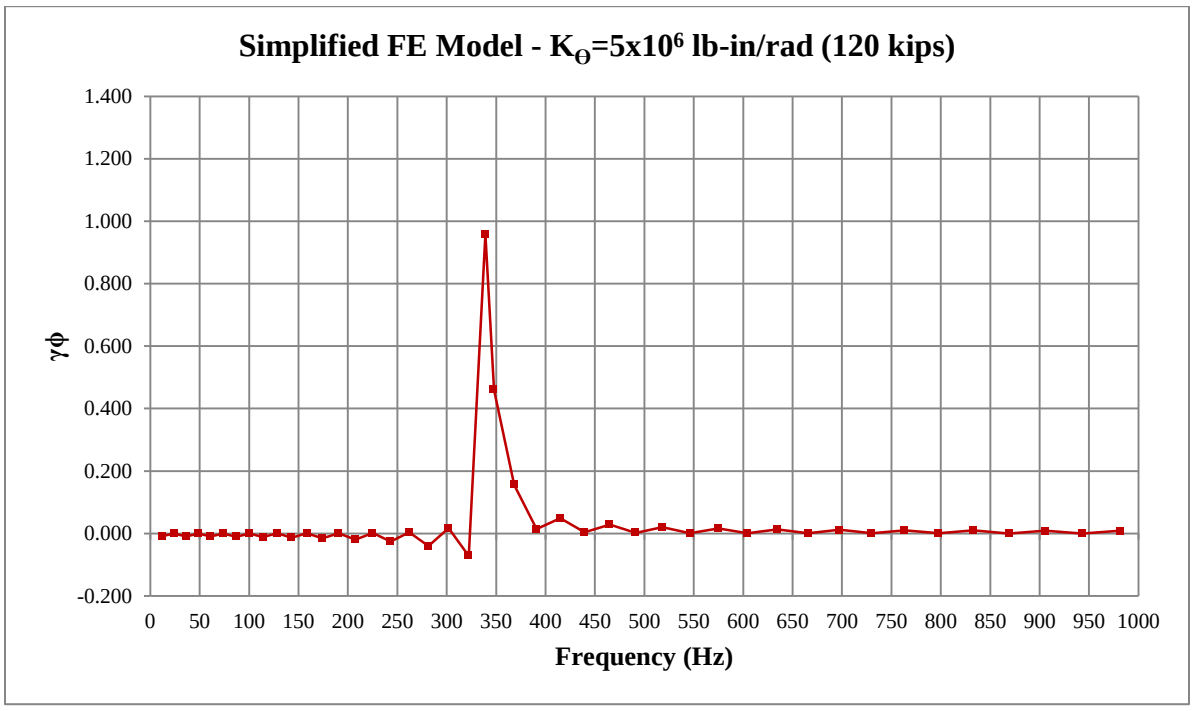

Figure 38: γϕ with respect to frequency for the K_Θ=5x10^6 lb-in/rad case at the 120 kip load level.

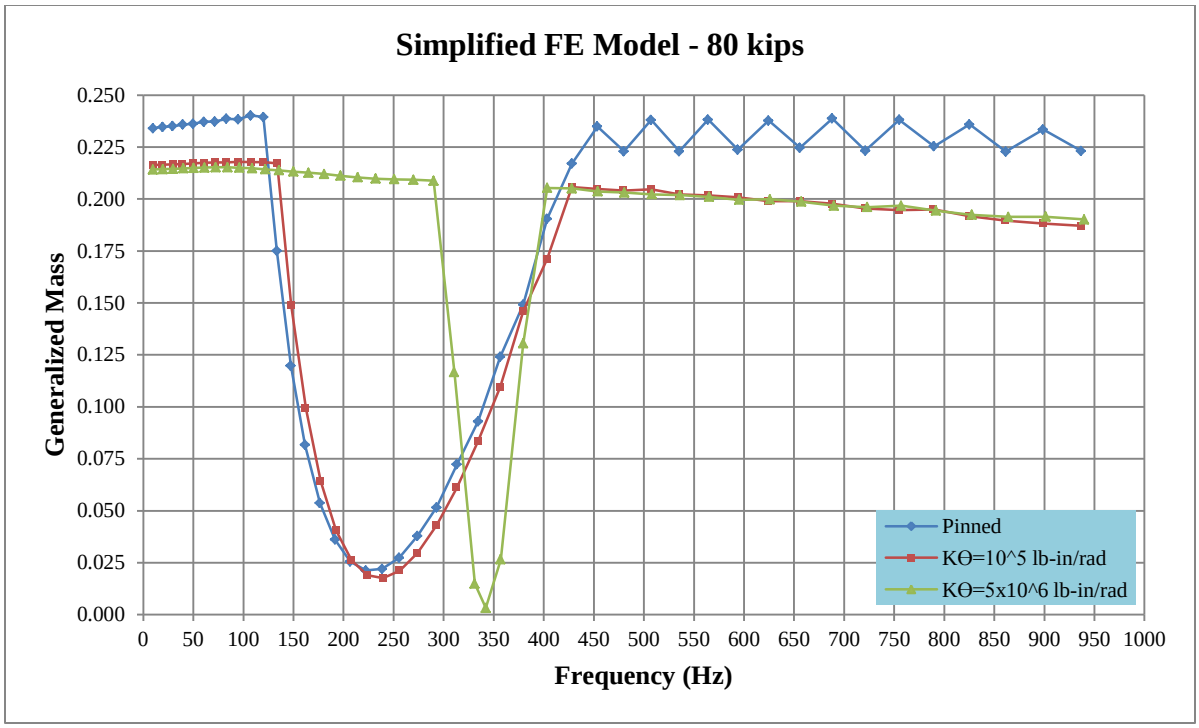

Figure 39: Generalized mass with respect to frequency for the 80 kip load level as K_Θ varies.

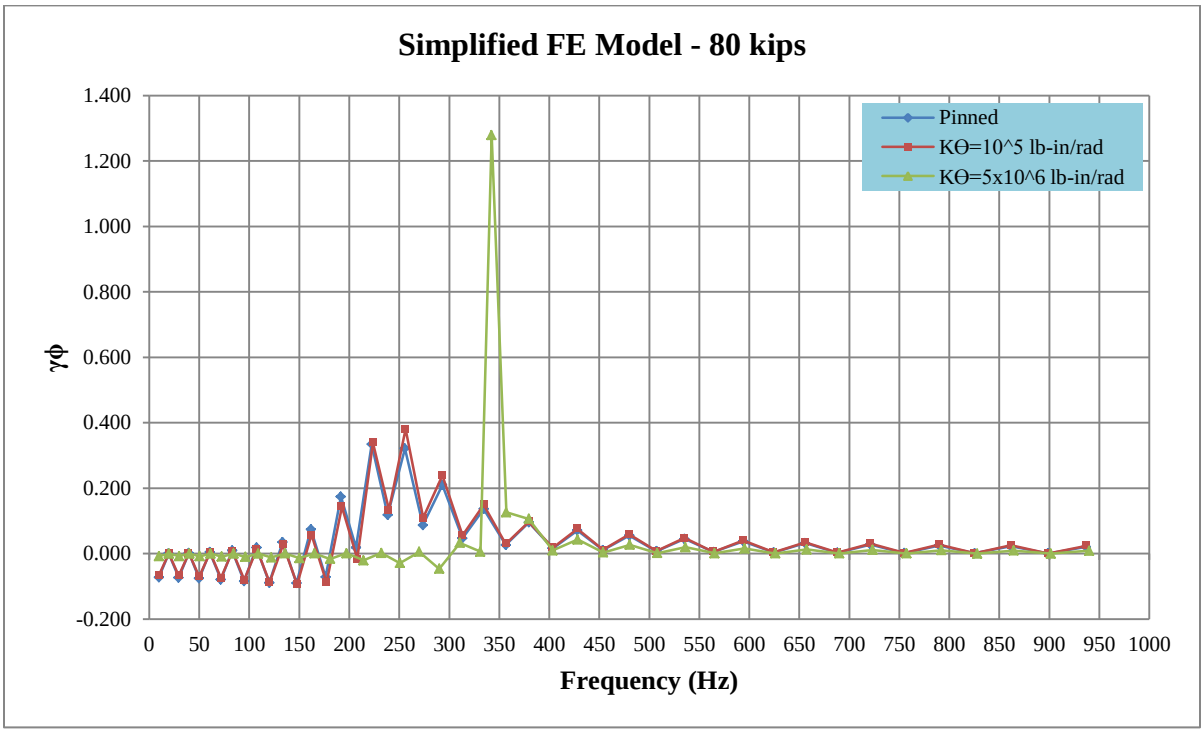

Figure 40: γϕ with respect to frequency for the 80 kip load level as K_Θ varies.

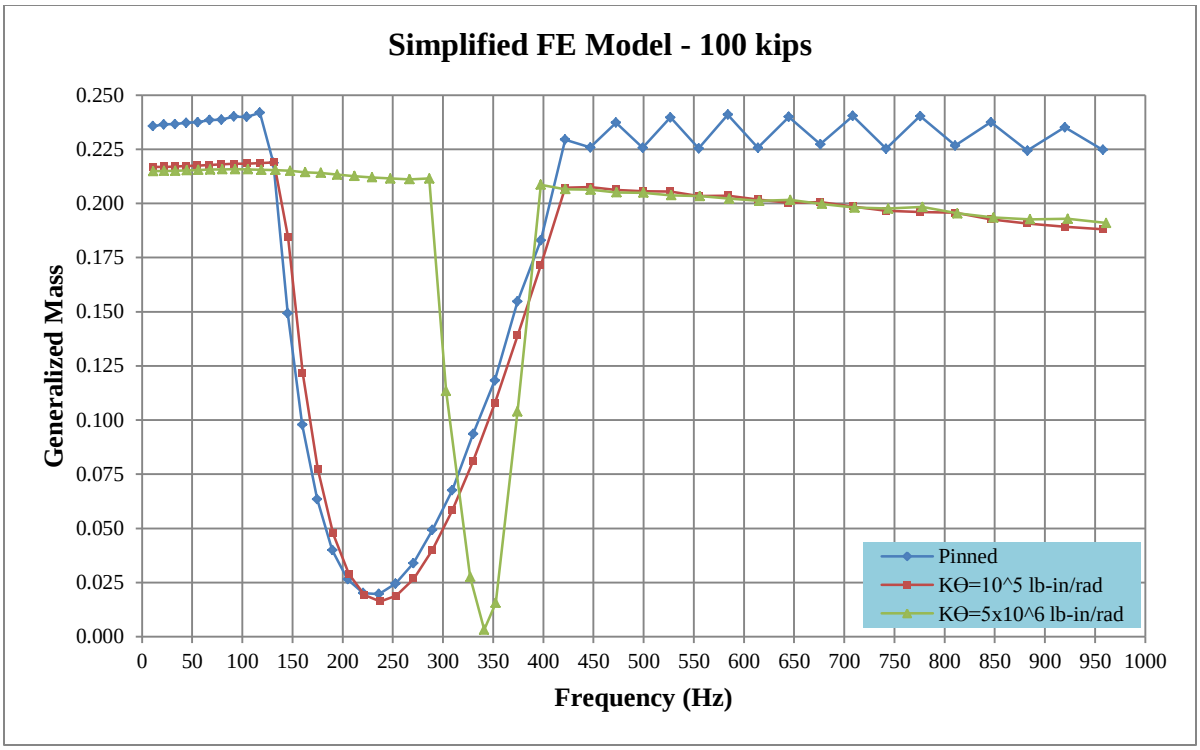

Figure 41: Generalized mass with respect to frequency for the 100 kip load level as K_Θ varies.

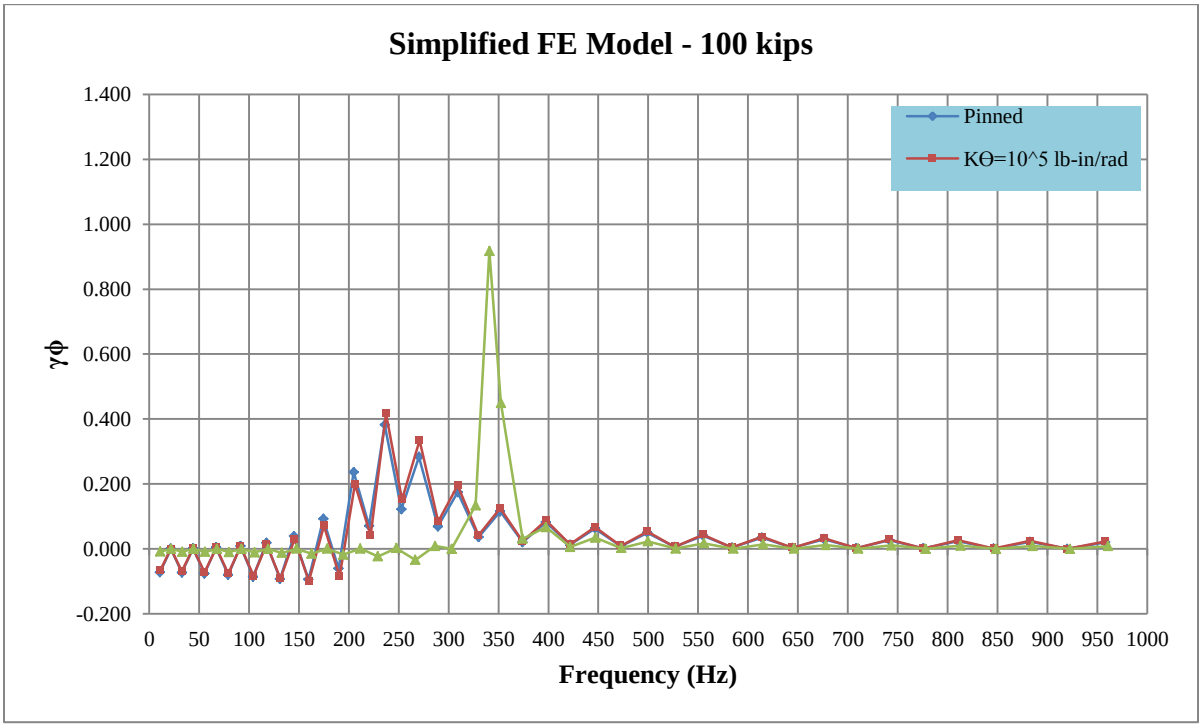

Figure 42: γϕ with respect to frequency for the 100 kip load level as K_Θ varies.

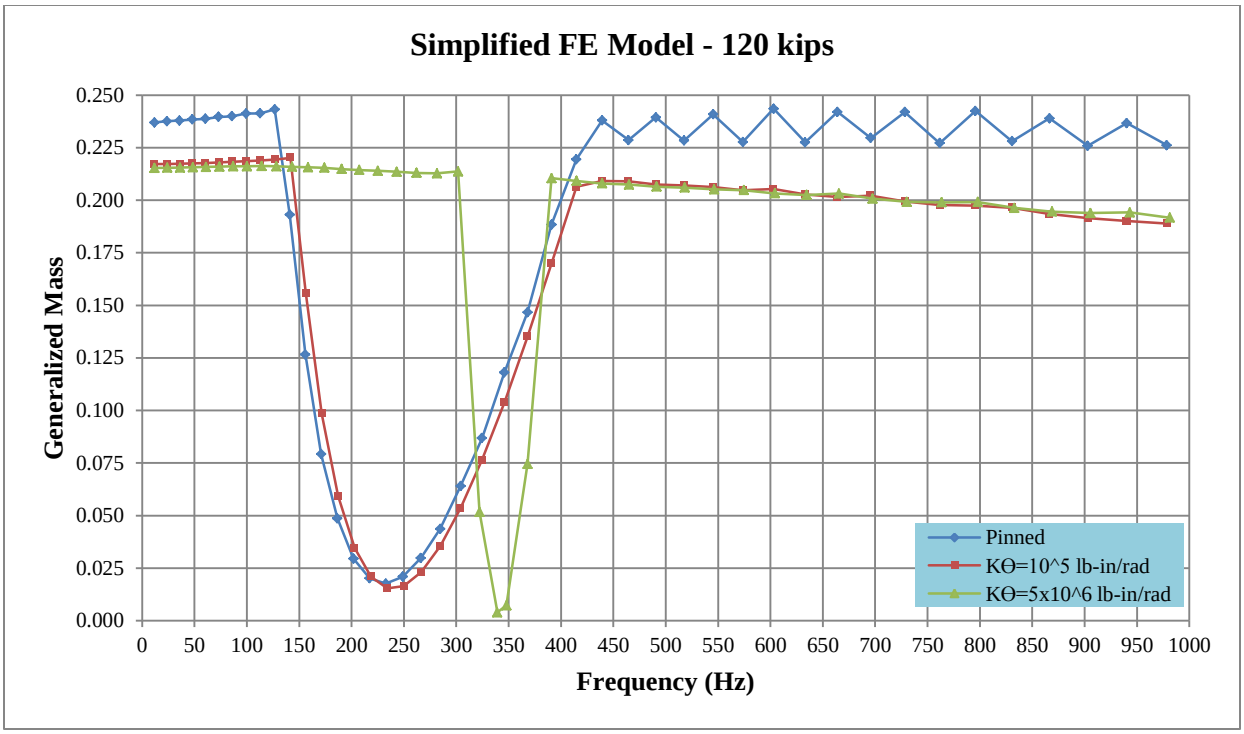

Figure 43: Generalized mass with respect to frequency for the 120 kip load level as K_Θ varies.

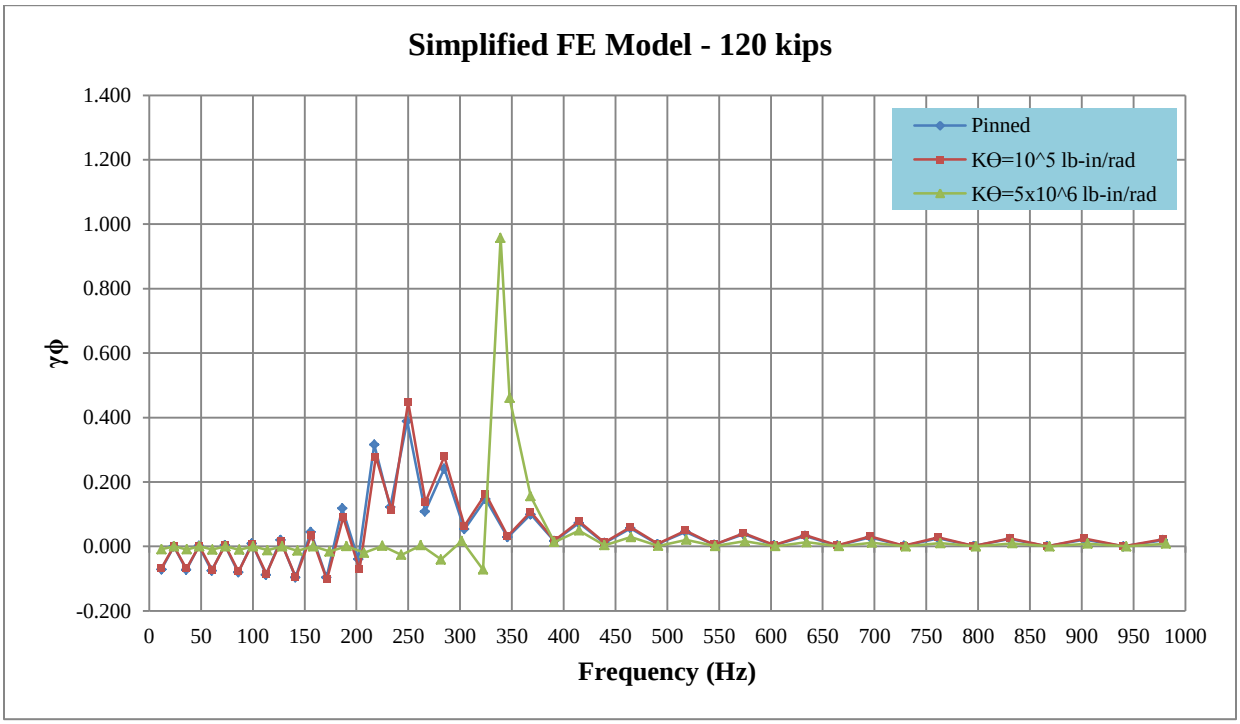

Figure 44: Comparison of γϕ with respect to frequency for the 120 kip load level as K_Θ varies.

Based on the data presented in Figure 27 through Figure 44, the following observations can be made concerning the relationship between load level, frequency, generalized mass, and $\gamma\phi$.

1. As K_Θ increases, the maximum $\gamma\phi$ value (amplification) occurs mostly in a single mode – herein called the significant mode. For low K_Θ values, multiple modes are significant with respect to the motion at the external end of the rod because multiple modes exhibit approximately the same amplification and these modes have frequencies which are closely spaced.
2. As load increases for low K_Θ values, the frequencies of the significant modes increase. However, for high K_Θ values, there is no correlation between frequency and load.
3. For high K_Θ values, there is a sharper increase in amplification and a sharper decrease in generalized mass than for low K_Θ values at the significant mode. As such, for high K_Θ values, the significant mode, which is the cantilever mode, can be identified based on this sharp change in amplification or generalized mass.

Chapter 7

SUMMARY AND CONCLUSIONS

Many dams have reached the end of their design lifetime and the structural integrity of the trunnion rods within some has become compromised based on recorded trunnion rod failures. As a result, there is a significant need to evaluate the structural integrity and existing tension within trunnion rods. The currently accepted means of evaluating the existing tension of a trunnion rod is lift-off testing, but it is hazardous, expensive, time consuming, and an undesirable long term solution. NDT, specifically, DW testing is viewed as a possible alternative to lift-off testing but it requires calibration with a FE model in order to estimate tension and past research has not yet fully calibrated a FE modeling method for the insert/grip nut anchorage mechanism. The goal of this study was to utilize the in-field data available for the DW testing for a specific dam in order to understand the behavior of the insert/grip nut anchorage mechanism. Based on the data presented in this study, this was accomplished through the completion of four objectives.

The first objective was to provide a detailed discussion on DW testing and existing work by other researchers on the corresponding finite element (FE) analysis. Through this discussion, the following conclusions were made:

1. Challenges such as inaccessibility to the interior (tension part) of the trunnion rod, additional factors affecting frequency other than tension, the inability to measure

some of the other factors affecting frequency, and the variability of the anchorage mechanism have prevented the widespread acceptance of the DW testing method.

2. The limitations of the existing FE model such as the excessively large computational resources required and the use of scanned parts have prevented the FE model from being capable of modeling exact field conditions of individual trunnion rods.

The second objective was to propose a new FE model of the trunnion rod utilizing the insert/grip nut anchorage mechanism based on the observations from an actual anchorage mechanism to overcome the limitations of the existing FE model. This was accomplished through the proposal of a FE model consisting of the following changes from the existing FE model:

1. Replacement of the scanned parts (grip nut and insert) of the existing FE model with smooth parts created within the FE software.
2. Simplification of the contact behavior between the insert and the rod, and the insert and the grip nut.
3. Reduction in the quantity of analysis steps.

The third objective was to confirm the validity of the proposed FE model by comparing the results with those from the DW test data for 10 different rods in which the tensile load is also known from the corresponding lift-off test. Based on these results, the following conclusions can be made:

1. The proposed FE model is capable of representing the DW test data with an error of 1.6% or less in 9 out of 10 cases.
2. A comparison between the proposed FE model and the classical fundamental frequency calculation for a cantilever beam revealed the pure cantilever is

consistently stiffer than the proposed FE model and the change in the fundamental cantilever frequency of the proposed FE model is very similar to the change in the fundamental cantilever frequency of the pure cantilever. This indicates the proposed FE model behaves similarly to the pure cantilever except that the rotational stiffness for the anchorage mechanism is not infinitely stiff (fixed condition).

3. The 1.5 hour runtime on a 16 core computer with 24 GB of RAM reveals demonstrates the improved efficiency of the proposed FE model compared to the existing FE model which had a 20.2 hour runtime on the same computer.

The final objective was to provide a simplified explanation of the behavior of the trunnion rod anchorage mechanism. Based on the result of the simplified FE model study, the following conclusions can be made regarding the behavior of the trunnion rod anchorage mechanism:

1. The anchorage mechanism can be represented with a K_θ at the anchorage point which is located at the location along the rod where the external end of the insert contacts the rod.
2. A rod with a K_θ less than 10^4 lb-in/radian behaves similarly to a rod with a pinned boundary condition while a rod with a K_θ greater than 10^9 lb-in/radian behaves similarly to a rod with a fixed boundary condition. Between these two values, the behavior of the rod varies between the two extreme boundary conditions.
3. A K_θ between 10^6 and 10^7 lb-in/radian (approximately $5x10^6$ lb-in/radian) is appropriate for the insert/grip nut anchorage mechanism presented in this study.

4. As K_θ increases, the maximum amplification of the cantilever end occurs mostly in a single significant mode. However, for low K_θ values multiple modes are significant and contain frequencies which are closely spaced.
5. As load increases for low K_θ values, the frequencies of the significant modes increase. However, there is no correlation between frequency and load for high K_θ values.
6. For high K_θ values, there is a sharper increase in amplification and a sharper decrease in generalized mass than for low K_θ values at the significant mode. As such, for high values, the significant mode, which is the cantilever mode, can be identified based on this sharp change in amplification or generalized mass.

7.1 Recommendations for Future Research

The results of the simplified FE model indicate that for a given rotational stiffness, provided its magnitude is sufficiently low, it is possible to detect a relationship between frequency and internal tension. As such, future research should be performed to test the rotational stiffness of a trunnion rod statically. Based on these test results, it may be possible to match the plot of $\gamma\phi$ vs. frequency for varying load levels to the DW test data to determine the internal tension level of the trunnion rod. Additionally, an experiment could be conducted to test the variability of rotational stiffness as load increases. The benefit of such an experiment would allow DW data and rotational stiffness data to be collected for known load levels, which would allow for calibration with a FE model.

REFERENCES

Abaqus. (2013). Abaqus Documentation. Providence, Rhode Island.

ASDSO (Association of State Dam Safety Officials). (2015). *Dam Safety 101*. Retrieved 2015, from http://www.damsafety.org/news/?p=e4cda171-b510-4a91-aa30-067140346bb2

Cesare, M. A., & Holt, J. D. (2012). Inspection of Trunnion Rod at Greenup Dam. *32nd Annual USSD Conference: Innovative Dam and Levee Design and Construction for Sustainable Water Management* (pp. 1237-1248). New Orleans: U.S. Society on Dams.

Cesare, M. A., Holt, J. D., & Guy, L. J. (2013). Integrity Testing of Pot-Tensioned Steel Trunnion Rods. *33rd Annual USSD Conference* (pp. 391-403). Phoenix: U.S. Society on Dams.

Cesare, M. A., Holt, J. D., Lindyberg, R. F., Lua, J. J., & Fang, X. (2013). Finite Element Modeling of Trunnion Rods. *33rd Annual USSD Conference: Changing Times-The Challenges and Risks of Managing Aging Infrastructure Under a New Financial Reality* (pp. 405-420). Phoenix: U.S. Society on Dams.

Cesare, M., & Holt, J. D. (2012a). *Patent No. 8,096,195.17.* USA.

Cesare, M., & Holt, J. D. (2012b). *Patent No. 8,176,800.15.* USA.

Ganelli, F., Beko, A., & Mordini, A. (2012, February). Structural Assessment of the Mignano Solid-Gravity Dam Based on the Monitoring Data. *Structural Engineering International, 22*, 130-139.

GOM. (2014, November 17). *ATOS Triple Scan - Revolutionary Scanning Technique*. Retrieved 2014, from Industrial 3D Measurement Techniques: http://www.gom.com/metrology-systems/system-overview/atos-triple-scan.html

Harrison, J. (2008, October 31). *Dams: History and Purpose*. Retrieved November 2014, from North West Power and Conservation Council: https://www.nwcouncil.org/history/DamsHistory

Herweynen, R. (2011). The integrity of old style post tensioned anchors in dams - a real dam safety issue. In J. Herweynen, A. J. Schleiss, & R. M. Boes (Eds.), *Dams and Reservoirs under Changing Challenges.* Boca Raton: Taylor & Francis Group, LLC.

Holt, D. J., & Cesare, M. A. (2010). *A Comparison of Flexural Wave and Side Sonic Testing for Determining Foundation Depth.* American Society for Nondestructive Testing.

Holt, J. D., & Cesare, M. A. (2012). Non Destructive Inspection of Existing Trunnion Rod Anchors. *USACE 2012 Locks Maintenance Workshop* (pp. 1-44). Washington, DC: U.S. Army Corps of Engineers (USACE).

Holt, J. D., Poiroux, G. V., Lindyberg, R. F., & Cesare, M. A. (2013). Detection Without Danger. *American Society of Civil Engineers*, 69-73,77.

ICOLD (International Commission on Large Dams). (2015, March 11). *Role of Dams*. Retrieved 2015, from http://www.icold-cigb.org/GB/Dams/role_of_dams.asp

Karnovsky, I. A., & Lebed, O. I. (2001). *Formulas for Structural Dynamics: Tables, Graphs, and Solutions.* New York, New York: McGraw-Hill.

Lynch, J. P., & Loh, K. J. (2006). *A Summary Review of Wireless Sensors and Sensor Networks for Structural Health Monitoring.*

NYSDEC (New York State Department of Environmental Conservation). (2014, November 7). *Inspection of Concrete Structures at Dams*. Retrieved November 2014, from http://www.dec.ny.gov/lands/67052.html

Poiroux, G. V. (2011). Post-Tensioned Trunnion Anchor Rod Testing, West Point Dam and R.F.Henry Dam. *31st Annual USSD Conference: 21st Century Dam Design-Advances and Adaptations* (pp. 459-476). San Diego: U.S. Society on Dams.

Poiroux, G. V., & Tashbin, D. (2009). Trunnion Anchor Rod Failures, West Point Dam Project. *29th Annual USSD Conference: Managing our Water Retention Systems* (pp. 73-84). Nashville: U.S. Society on Dams.

Schaff, D. (2009). *Tainter Gate Trunnion Anchorage: Database of Inspection, Testing, and Incidents.* IWR, Risk Management Center.

Triana, E., Escuder, I., de Membrillera, M., & Altarejos, L. (2006). Dam failure consequences on water resources system. In L. Berga, J. Buil, E. Bofill, J. De Cea, J. Garcia Perez, G. Manueco, . . . J. Yague (Eds.), *Dams and reservoirs, Societies and Environment in the 21st Century* (pp. 357-363). Boca Raton: Taylor & Francis Group, LLC.

USACE (U.S. Army Corps of Engineers). (2000). *Design of Spillway Tainter Gates.* EM 1110-2-2702.

USACE (U.S. Army Corps of Engineers). (2014). *Design of Hydraulic Steel Structures.* ETL 1110-2-584.

USACE (U.S. Army Corps of Engineers). (2015). *National Inventory of Dams*. Retrieved 2015, from CorpsMap: http://geo.usace.army.mil/pgis/f?p=397:1:0

USDHS (U.S. Department of Homeland Security). (2011). *Dams Sector: Estimating Economic Consequences for Dam Failure Scenarios.* Retrieved November 2014, from http://www.damsafety.org/media/documents/owner%20documents/Dam%20Security/Dams%20Sector%20-%20Consequence%20Estimation%20-%20Economic%20Consequences.pdf

USGS (U.S. Geological Survey). (2014, September 30). *The National Map Small-Scale Collection*. Retrieved November 2014, from www.nationalatlas.gov